EARTH SURFACE PROCESSES AND LANDFORMS
Earth Surf. Process. Landforms (2016)

Published online in Wiley Online Library
(wileyonlinelibrary.com) DOI: 10.1002/esp.3874

Relations between rainfall–runoff-induced erosion and aeolian deposition at archaeological sites in a semi-arid dam-controlled river corridor

Brian D. Collins,[1]* David R. Bedford,[1] Skye C. Corbett,[1] Collin Cronkite-Ratcliff[1] and Helen C. Fairley[2]
[1] US Geological Survey, Menlo Park, CA, USA
[2] US Geological Survey, Grand Canyon Monitoring and Research Center, Flagstaff, AZ, USA

Received 30 October 2014; Revised 20 November 2015; Accepted 23 November 2015

*Correspondence to: Brian D. Collins, US Geological Survey, 345 Middlefield Rd, MS973, Menlo Park, CA 94025, USA. E-mail: bcollins@usgs.gov

ESPL
Earth Surface Processes and Landforms

ABSTRACT: Process dynamics in fluvial-based dryland environments are highly complex with fluvial, aeolian, and alluvial processes all contributing to landscape change. When anthropogenic activities such as dam-building affect fluvial processes, the complexity in local response can be further increased by flood- and sediment-limiting flows. Understanding these complexities is key to predicting landscape behavior in drylands and has important scientific and management implications, including for studies related to paleoclimatology, landscape ecology evolution, and archaeological site context and preservation. Here we use multi-temporal LiDAR surveys, local weather data, and geomorphological observations to identify trends in site change throughout the 446-km-long semi-arid Colorado River corridor in Grand Canyon, Arizona, USA, where archaeological site degradation related to the effects of upstream dam operation is a concern. Using several site case studies, we show the range of landscape responses that might be expected from concomitant occurrence of dam-controlled fluvial sand bar deposition, aeolian sand transport, and rainfall-induced erosion. Empirical rainfall-erosion threshold analyses coupled with a numerical rainfall–runoff–soil erosion model indicate that infiltration-excess overland flow and gullying govern large-scale (centimeter- to decimeter-scale) landscape changes, but that aeolian deposition can in some cases mitigate gully erosion. Whereas threshold analyses identify the normalized rainfall intensity (defined as the ratio of rainfall intensity to hydraulic conductivity) as the primary factor governing hydrologic-driven erosion, assessment of false positives and false negatives in the dataset highlight topographic slope as the next most important parameter governing site response. Analysis of 4+ years of high resolution (four-minute) weather data and 75+ years of low resolution (daily) climate records indicates that dryland erosion is dependent on short-term, storm-driven rainfall intensity rather than cumulative rainfall, and that erosion can occur outside of wet seasons and even wet years. These results can apply to other similar semi-arid landscapes where process complexity may not be fully understood. Copyright © 2015 John Wiley & Sons, Ltd.

KEYWORDS: sediment transport; erosion; runoff; archaeological; Grand Canyon

Introduction

Erosion of semi-arid hillslopes through rainfall–runoff is a well-studied process with important implications to many landscapes (e.g. Blackburn, 1975; Fitzjohn *et al.*, 1998; Canfield *et al.*, 2001; Castillo *et al.*, 2003; Cantón *et al.*, 2011). Similarly, aeolian transport is also a significant process in semi-arid regions (e.g. Breshears *et al.*, 2003; Okin *et al.*, 2006; Nickling and Neuman, 2009), although its effects on mitigating runoff-induced erosion have received comparatively less attention (e.g. Bullard and Livingstone, 2002; Sankey and Draut, 2014). In certain instances, and particularly within semi-arid fluvial landscapes where infrequent storms trigger widespread gullying and micro-climates cause preferential aeolian transport, both of these processes can interact to affect landscape response (Belnap *et al.*, 2011). This is particularly true where fluvial systems undergo fluctuating flow conditions, thereby allowing sand bars to form with subsequent aeolian sand transport to adjacent hillslopes. Sand deposits may then protect underlying substrates from erosion. The system may become even more complex if the fluvial system is affected by anthropogenic effects such as dams (Draut, 2012). These may then block fluvial sediment transport altogether and/or affect base-level flow of tributaries.

The confluence of these processes is much more than an academic study. Instead, it is critically important to understanding the depositional histories of arid and semi-arid environments worldwide (e.g. Roskin *et al.*, 2013). Perhaps nowhere are these studies more relevant than for studying the context and fate of many areas of archaeological interest. Evidence of prehistoric human occupation is often found in river valleys where a combination of fluvial, alluvial and aeolian deposition preserves artifacts, structures, and other cultural features (e.g. Russia – Holliday *et al.*, 2007; India – Gibling *et al.*, 2008; Argentina – Martínez and Martínez, 2011; Israel – Roskin *et al.*, 2014). Whereas the depositional environment that preserves archaeological sites is important for understanding their cultural context (e.g. Harris, 1989; Waters, 1997), erosional processes are often responsible for the initial discovery of sites. However, modern-day erosion can also threaten any future interpretation by displacing or entirely removing artifacts from their original depositional context

(Wainwright, 1994). Here we study these processes as they relate to archaeological site preservation in Grand Canyon, Arizona, USA (Figure 1) where hundreds of archaeological sites are located within aeolian- and fluvial-derived substrates in close proximity to the dam-controlled, sediment-limited Colorado River (Figure 2), and where erosion of sites through gullying currently threatens site integrity (Fairley, 2003, 2005; Draut and Rubin, 2008; Draut *et al.*, 2008).

Our investigation aims to sort out the competing and controlling characteristics of coupled fluvial–aeolian–runoff interactions in a semi-arid landscape with the purpose of determining the range of possible geomorphic responses from precipitation and aeolian processes. As motivation for our studies, we begin by providing a brief synopsis of dam management and effects as they apply to archaeological site change along the Colorado River corridor in Grand Canyon. Then, using 4+ years (2006–2010) of measured topographic changes at 13 archaeological sites located throughout the river corridor, we analyze both the topographic changes (to identify short-term trends) and the proxies for these changes, whether from rain-fall runoff or aeolian transport. Combining this data with site-specific meteorological measurements, we formulate a process-based empirical threshold model to distinguish sediment transport (i.e. erosion) caused by different runoff modes (i.e. infiltration-excess versus saturation-excess overland flow). We further use false-positives and false-negatives from the empirical threshold equations to identify additional likely influences on sediment transport. Threshold results are verified using a two-dimensional rainfall–runoff model and compared to long-term precipitation records to identify the likely return period of erosion-inducing storms in this landscape. Finally, we use examples from the data to showcase three distinct possible responses – negative (erosion), mixed, and positive (net deposition) – that should be considered when predicting dryland site change resulting from the net effect of fluvial–aeolian–alluvial interactions.

Whereas the numerical model requires a detailed knowledge of topography and substrate properties to implement, the empirical model can be easily applied to identify short-timescale landscape response in other semi-arid environments where only generalized substrate and weather data are available. Thus, although our research is conducted within the context of archaeological site management, both the methods and results are applicable to a wide range of semi-arid landscapes, where assumed complexities in sediment transport processes might otherwise preclude first-order analysis and interpretation.

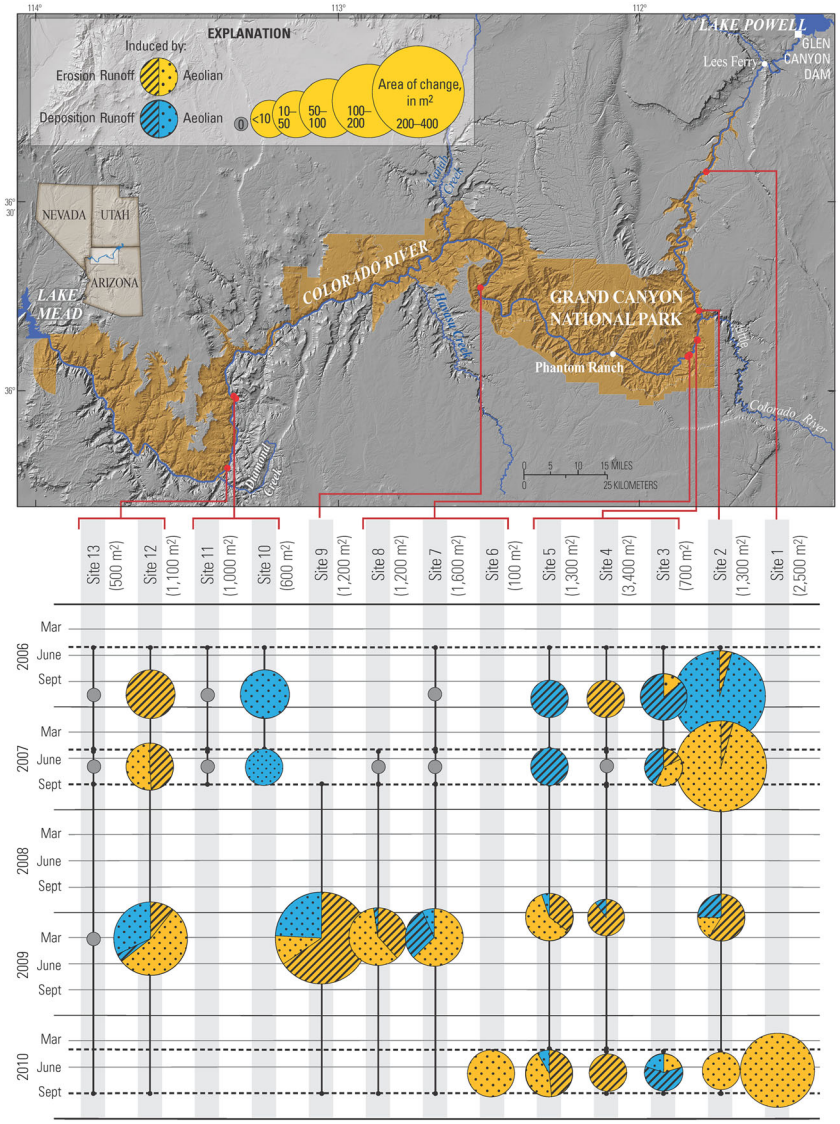

Figure 1. Regional map of Grand Canyon National Park showing the 13 sites referenced in this investigation and the associated change detected at each site between May 2006 and September 2010. Pie chart size indicates the total area of erosion and deposition. Hatching pattern indicates the primary geomorphic process presumed to have caused the change. Average total area where change detection was investigated at each site is indicated in parentheses. Dashed lines are dates of data collection; pie chart locations indicate measured change between the adjacent dashed lines. This figure is available in colour online at wileyonlinelibrary.com/journal/espl

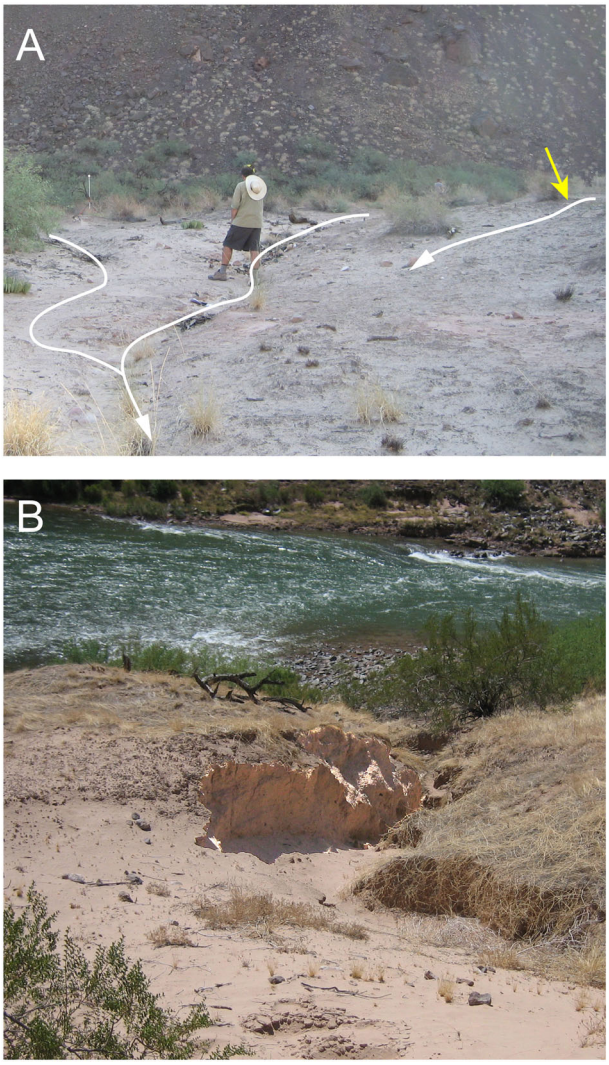

Figure 2. Erosion of archaeological sites in Grand Canyon from gullying at (A) site 5 and (B) site 12. Erosion in all gullies at (A) occurred over a five-year monitoring period (2006–2010), most dramatically in the southern-most gully (yellow arrow – see Figure 3). Erosion at (B) now threatens archaeological resources previously buried by aeolian sediments (foreground) and exposed in the 1-m-deep cutbank. This figure is available in colour online at wileyonlinelibrary.com/journal/espl

Archaeological Site Erosion Along the Colorado River Corridor of Grand Canyon, Arizona, USA

Grand Canyon is among the world's most iconic landscapes, showcasing 1.8 billion years of geological history (e.g. Billingsley, 2000) and classic examples of fluvial geomorphology (e.g. Howard and Dolan, 1981). During the last 11 000 years, humans have left their imprint at numerous locations along the Colorado River in Grand Canyon (e.g. Powell, 1875; Taylor, 1958; Schwartz, 1965; Jett, 1968; Fairley, 2003; Pederson *et al.*, 2011). Some evidence of past human habitation is preserved by archaeological sites situated in and on aeolian dune-covered fluvial terraces (i.e. source-bordering dunes) (Bullard and McTainsh, 2003) adjacent to the Colorado River (Fairley *et al.*, 1994). Aeolian deposits at some sites can be tens to hundreds of centimeters thick (Draut *et al.*, 2008; Hereford *et al.*, 2000), similar to other archaeologically important areas located in the semi-arid American southwest (e.g. Drakos and Reneau, 2007). Because these sites contain valuable information about the past and serve as tangible evidence of Native Americans' prehistoric use of this area, the physical processes contributing to their preservation or degradation within the Colorado River corridor of Grand Canyon National Park is a subject of considerable interest. Uncertainty surrounding the flow-limiting and sediment-blocking effects of Glen Canyon Dam (Topping *et al.*, 2000, 2003), located 25 km upstream from Grand Canyon, on the stability of these archaeological sites provides additional incentive to understand the diverse factors contributing to the preservation and erosion of these non-renewable cultural resources.

Topographic change resulting from a variety of natural processes is typical in the high-relief, semi-arid Grand Canyon region. Intense precipitation, which commonly accompanies the monsoon-type summer weather systems in Arizona, can cause rapid erosion of many desert substrates via overland flow and gullying (e.g. Pederson *et al.*, 2006a; O'Brien and Pederson, 2009a) (Figure 2). High-velocity winds also change landscapes by transporting sand both to and from archaeological sites (e.g. Draut and Rubin, 2008). The first observations of potentially exacerbated gully erosion at archaeological sites below Glen Canyon Dam (Hereford *et al.*, 1993) coincided with a series of high-flow experimental releases (termed HFEs) in the early 1980s which set the stage for a suite of investigations aimed at understanding the interactions between dam operations and archaeological site erosion (Thompson and Potochnik, 2000; Fairley, 2003; Pederson *et al.*, 2006a; Draut and Rubin, 2008). The earliest investigations suggested that increased archaeological site erosion is tied to tributary base-level lowering resulting from decreased channel margin deposition by regulated river flows compared with pre-dam flood levels (Hereford *et al.*, 1993). It was subsequently proposed that flows above the level of those typically used for power generation from the dam (i.e. HFEs> 637 m^3/s) might result in a reduction of gully knickpoint migration by infilling the lowest parts of the gully systems (Thompson and Potochnik, 2000). However, field tests were inconclusive (Hazel *et al.*, 2008) and potentially irrelevant, as might have been predicted based on the findings of Hereford *et al.* (1993), given that the HFE flow levels were well below those of pre-dam flows.

Thompson and Potochnik (2000 recognized that decreases in the amount of aeolian surface deposits resulting from the supply-limiting effects of the upstream dam could be a critical factor contributing to erosion of cultural sites located on the banks of the post-dam Colorado River. Comprehensive research on long-term solutions to gully erosion via the aeolian effects of HFEs was initiated in 2003 and identified the types of landscapes that might be restored by dam operations (Draut and Rubin, 2008; Draut *et al.*, 2008; Draut, 2012). Draut (2012 concluded that landscapes with a high potential for restoration, designated as modern-fluvial-sourced (MFS) aeolian deposits, must be located downwind from fluvial sand bars that are periodically replenished by sediment-rich high flows under the post-dam flow regime. MFS deposits are differentiated from relict-fluvial-sourced (RFS) deposits (Draut and Rubin, 2008; Draut, 2012) which do not receive new aeolian sand supply because they are not situated downwind of modern (post-dam construction) sandbars formed by large (>1160 m^3/s) restorative floods below Glen Canyon Dam (Wright *et al.*, 2005).

Despite evidence for linkages between fluvial and related aeolian processes (Draut *et al.*, 2010a; Draut, 2012; Sankey and Draut, 2014) and the potentially restorative sand deposition and site burial effects to archaeological sites located in the river corridor, quantitatively separating the natural factors contributing to site erosion (e.g. precipitation-induced gullying) from those potentially related to dam operations (e.g. reduction in the volume, elevation and distribution of sand bars) has been difficult. Studies that conclusively link archaeological site change to specific natural or anthropogenic causes are lacking due to the complexities involved in identifying the main drivers behind particular processes in such heterogeneous landscapes. The present study makes headway in this direction by exploring and presenting generalized

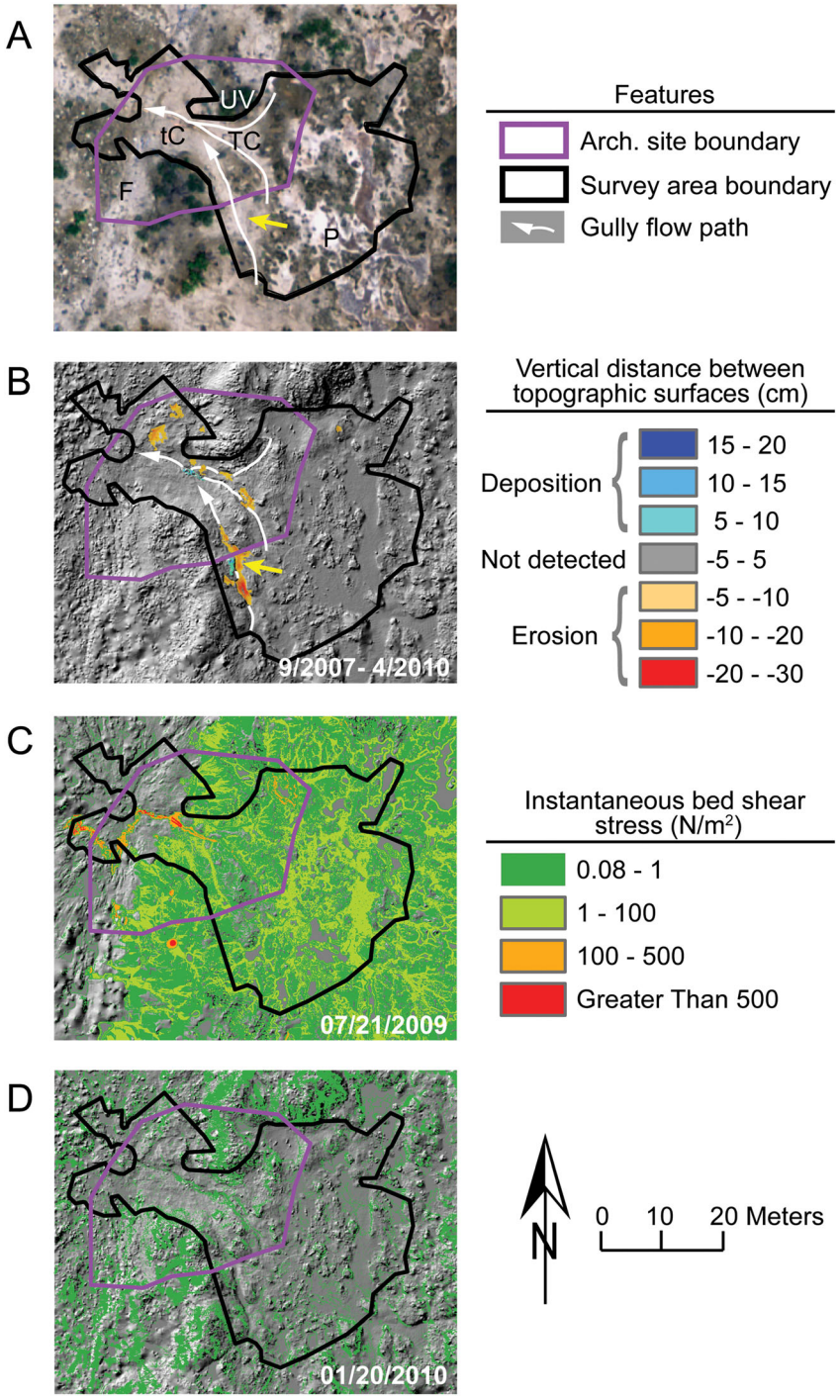

Figure 3. (A) Aerial photograph of site 5. Labels indicate typical substrate type – see Table I. (B) Topographic change observed between September 2007 and April 2010 within the survey area boundary. (C, D) Modeled runoff-generated bed shear stress for storms with high (C) and low (D) normalized intensity (*I*) during this time period. In (B), only change areas touching a gully flow path are due to runoff; others are from aeolian processes. Location of yellow arrow in (A, B) coincides with that shown in Figure 2A. Runoff is concentrated in areas with low infiltration capacity (i.e. the playa and biological soil crust areas). Fluvial terrace areas to the northwest have low runoff and bed shear stress, except where gullies concentrate the flow. This figure is available in colour online at wileyonlinelibrary.com/journal/espl

relationships between rainfall–runoff erosion and aeolian deposition based on a number of site-specific cases, but representative of possibilities in coupled fluvial–aeolian landscapes worldwide.

Methods

Study areas

We selected 13 archaeological site study areas distributed throughout the 446 km length of the Colorado River corridor (Figure 1) for in-depth analysis and modeling. The sites exhibit a range of geomorphic settings, substrate characteristics, and surface processes commonly observed within Grand Canyon (see Collins *et al.*, 2009, 2012), and they include sites both with and without engineered erosion-control features (e.g. rock and brush check dams) (see Pederson *et al.*, 2006a). All are located on either alluvial deposits or former (pre-dam) fluvial terraces within 200 m of the river's edge as measured at current low-flow (i.e. 230 m^3/s) water levels. Watershed areas vary between 1400 and 61 400 m^2 and are composed of a variety of substrates ranging from aeolian sand, to biological soil-crusted

Table I. Site drainage area, slope, substrate, and infiltration data.

Site #	Arizona archaeological site ID#[a]	Up-terrace drainage area (m^2)	Average slope, β (°)	Predominant substrates[b] (%)	Site area hydraulic conductivity $K_{G\text{-}A}$ average[c] (m/s)	Effective substrate porosity, θ_e	Effective subsurface depth, z_e (m)
1	AZ:C:05:0031	21,000	8	C(39), A(36), AS(13), TC(11) UV(1)	5.7E-5	0.28	13.2
2	AZ:C:13:0006	4,600	19	C(54), TC(34), UV(8), AS(4)	1.8E-5	0.22	9.4
3	AZ:C:13:0099	61,400	6	C(61), F(18), P(9), tC(6), B(3), UV(3)	1.3E-5	0.22	1.7
4	AZ:C:13:0099p	34,900	<1	C(69), P(13), T(6), B(6), tC(5), UV(1)	9.9E-6	0.10	3.7
5	AZ:C:13:0336	3,900	6	tC(32), TC(26), UV(18), F(13), P(11)	1.2E-5	0.22	2.5
6	AZ:C:13:0321	1,500	6	UV(39), AS(37), TC(24)	1.2E-5	0.28	2.6
7	AZ:C:13:0346	6,900	12	A(67), TC(21), UV(11), F(1)	2.4E-5	0.22	6.8
8	AZ:C:13:0348	3,800	12	A(74), TC(16), UV(6), F(4)	2.6E-5	0.22	6.8
9	AZ:B:10:0225	24,700	20	C(87), AS(12), A(1)	1.5E-5	0.28	2.2
10	AZ:G:03:0041	7,900	23	C(69), TC(16), UV(12), AS(3)	2.5E-5	0.18	10.2
11	AZ:G:03:0002	23,700	5	C(66), TC(24), UV(10)	1.9E-5	0.18	8.2
12	AZ:G:03:0072US	6,400	14	A(37), AS(28), TC(20), UV(15)	2.6E-5	0.18	14.1
13	AZ:G:03:0072DS	1,400	24	A(56), TC(36), UV(8)	2.5E-5	0.18	15.1

[a]Designation is for archaeological site reference using standard protocols used in Arizona, USA.
[b]A = alluvium, AS = aeolian sand, B = bedrock, C = colluvium, F = fluvial terrace, TC = thick biological soil crust, tC = thin biological soil crust, P = playa, UV = under vegetation.
[c]Values have been multiplied by 0.3 to represent the Green–Ampt infiltration parameter ($K_{G\text{-}A}$).

fluvial sediments, to bedrock (Table I). Most sites are founded on gentle sloping terrace surfaces (as delineated by the average slope, β, Table I; e.g. Figure 2A), although some are located predominantly on and within steep terrace risers (e.g. Figure 2B). Nearly all sites are traversed by several shallow gullies less than 0.5 m in depth; some gullies contain knickpoints that act as loci for erosion. Many gullies currently threaten the integrity of archaeological resources that include masonry structures, artifact scatters, and roasting pits dating approximately to between 900 and 1800 CE. Vegetation is typical for the desert southwest, with interspersed cacti varieties and mesquite trees, along with smaller shrubs and grasses. We provide additional site specific geomorphological descriptions in Collins *et al.* (2009, 2012).

Terrestrial LiDAR monitoring

We collected repeat-sets of terrestrial LiDAR (light detection and ranging) data at the 13 archaeological sites in May 2006, May 2007, September 2007, April 2010, and September 2010 (Figure 1) using tripod-mounted Riegl Z210 and Z420i time-of-flight-type laser instruments georeferenced with total station and global positioning system (GPS) measurements. High-resolution bare-earth point clouds (with typical point density of 96 points/m^2) and surface models (with 5 cm grid size) of each site, ranging in total surface area between 100 m^2 and 3400 m^2 (averaging 1300 m^2; Figure 1), were constructed following a suite of filtering, registration, georeferencing, and surface building algorithms (Collins *et al.*, 2009, 2012). The resultant point cloud accuracy is between 1.5 and 4 cm, with temporally consecutive absolute surface model change detection thresholds ranging from 3 cm (for the Z420i data) to 8 cm (for the Z210 data). We computed areas between 0.02 m^2 and 260 m^2, and volumes ranging from 0.001 m^3 to 62 m^3, of eroded and deposited sediment over 5 to 32 month intervals by comparing sequential pairs of surface models at each site (e.g. Figure 3B). We determined the likely mode of sediment transport as from either runoff or aeolian processes by observation of the location and geomorphic settings of the deposits (Collins *et al.*, 2009, 2012). Areas exhibiting change were determined to be from runoff if they showed evidence of alluvial transport (e.g. downward fining of deposited sediment, presence of erosive cutbanks) and spatial distributions coincident with either existing or incipient gullies. Likewise, areas showing evidence of wind transport (e.g. ripples, dunes) and/or larger spatial distributions coincident with uniform sand deposits compared to smaller and gully-aligned alluvial change areas were determined to be from an aeolian process mode of transport. Interpretations were based on site observations and documentation provided in Collins *et al.* (2009, 2012). We re-evaluated original interpretations from these studies for two sites (sites 5 and 6) in light of new analyses indicating more conclusive evidence for a precipitation/runoff related trigger for documented site erosion during the May 2006–September 2007 and April 2010–September 2010 time periods, respectively.

Weather data collection and analysis

A series of automated weather stations operating in Grand Canyon between 2006 and 2010 provided precipitation and wind data for our analyses. We coalesced and integrated data from several field studies (Draut *et al.*, 2009a, 2009b, 2010b; O'Brien and Pederson, 2009b; Dealy *et al.*, 2014) to build continuous time series for analysis and corroboration with documented site changes. These data provide the highest resolution data (with four-minute sampling intervals) ever collected at the bottom of Grand Canyon. Episodic weather station equipment failure at some sites necessitated substituting precipitation data from neighboring (secondary) weather stations along the river corridor. With these substitutions, our overall data coverage for all time periods exceeds 80% at all sites (Table II). During only one time period at two sites (May 2006 to May 2007 at sites 7 and 8) is the temporal coverage less than 80%; we do not include analyses for these cases. For the remainder of the sites with incomplete

Table II. Location and temporal coverage of precipitation data used for intensity-storm total analyses.

Site #	Distance to primary weather station (km)	Distance to secondary weather station (km)	Average temporal coverage of primary data for all monitoring periods	Average temporal coverage of primary and secondary data for all monitoring periods
1	0	0	100%	100%
2	0	3	80%	96%
3	0	6	71%	96%
4	0	6	71%	96%
5	0	6	71%	96%
6	1	6	100%	100%
7	0	6	79%	81%[a]
8	0	6	79%	81%[a]
9	12	n/a	100%	100%
10	8	21	36%	86%
11	9	21	37%	87%
12	0	29	80%	96%
13	0	29	80%	96%

[a]Data coverage during May 2006–May 2007 is only 18% and not used for analysis.

records, ranges of missing data are generally not coincident with typical times of heavy precipitation in the canyon (i.e. during the summer monsoon from July through September or the Pacific storm winter season from November through March).

To generate intensity relationships for individual storm events, we identified storms as continuous periods of time with rainfall separated by more than six continuous hours of no rain; this threshold has also been used in identifying debris-flow-generating storms (Deganutti *et al.*, 2000). We chose the maximum 10-minute intensity to be a good measure of storm runoff potential – rates lower than this were deemed to be too short and disjointed for causing significant runoff and those larger were determined to overly smooth potentially important periods of heavy rainfall. To compute the maximum 10-minute intensity, we resampled the four-minute data at evenly-divided one-minute resolution and calculated the maximum 10-minute moving sum. As proxies for the conditions that generate overland flow and channelized erosion at the sites, we interrogated these results to identify storms (Table III) with the highest 10-minute intensity and the largest total precipitation during each LiDAR monitoring period. Storm rainfall intensities and totals reached 107 mm/h and 45 mm, respectively, at some sites during the monitoring period, and were typically coincident with the summer monsoon. We generated expected recurrence intervals for all storms by comparing their corresponding daily total precipitation to records (NOAA, 2013) from the only two long-term (75+ year) rain gages located at river level in Grand Canyon (Lees Ferry and Phantom Ranch, located between 22 and 195 km from the archaeological sites; Figure 1).

For sites in which aeolian deposition can potentially influence archaeological site stability, we determined the range of required wind transport directions by measuring the horizontal

Table III. Monitoring-period-specific storm attributes and recurrence intervals for sites experiencing runoff and erosion.

Site #	Time period	Storm date	Peak 10-minute storm intensity (mm/h)	Storm precipitation total (mm)	Daily precipitation total (mm)	Daily total precipitation recurrence interval at Lees Ferry[a] (years)	Daily total precipitation recurrence interval at Phantom Ranch[b] (years)
2	May 2006–May 2007	August 24, 2006	42	9	9	0.2	0.1
2	May 2007–September 2007	July 30, 2007	41	17	17	0.9	0.4
2	September 2007–April 2010	July 6, 2008	107	23	23	1.8	0.9
3	May 2006–May 2007	August 24, 2006[c]	42	9	9	0.2	0.1
3	May 2007–September 2007	July 30, 2007	51	17	17	0.9	0.4
3	April 2010–September 2010	August 6, 2010	46	13	13	0.5	0.3
4	May 2006–May 2007	August 24, 2006[c]	42	9	9	0.2	0.1
4	September 2007–April 2010	July 20, 2009	76	27	27	3.6	1.4
4	April 2010–September 2010	August 6, 2010[c]	46	13	13	0.5	0.3
5	May 2006–May 2007	August 24, 2006[c]	42	9	9	0.2	0.1
5	May 2007–September 2007	July 30, 2007[c]	51	17	17	0.9	0.4
5	September 2007–April 2010	July 20, 2009[c]	76	27	27	3.6	1.4
5	April 2010–September 2010	August 6, 2010[c]	46	13	13	0.5	0.3
6	April 2010–September 2010	August 6, 2010	47	10	10	0.2	0.1
7	September 2007–September 2010	May 22, 2009	86	45	31	5.2	2.0
8	September 2007–September 2010	May 22, 2009[c]	86	45	31	5.2	2.0
9	September 2007–September 2010	May 22, 2009	86	45	37	8.3	3.4
12	May 2006–May 2007	August 11, 2006	57	39	39	13.8	4.8
12	May 2007–September 2007	July 29, 2007	74	31	32	5.9	2.0
12	September 2007–September 2010	August 27, 2010	53	13	13	0.4	0.3

[a]Lees Ferry analysis based on 86.4% data coverage (Hereford *et al.*, 2014) over 96 years (1916–2012).
[b]Phantom Ranch analysis based on 90.4% data coverage (Hereford *et al.*, 2014) over 78 years (1935–2012).
[c]Denotes duplicate storms represented at nearby sites and not used for seasonal statistical analyses.

angle between nearby river sand bars and dunes (i.e. sand sources) and the archaeological sites. We then analyzed available wind and sand transport data and interpretations (Draut *et al.*, 2009a, 2009b, 2010b) to identify whether sand could have been transported to the archaeological sites when new aeolian sand deposition was identified in the change detection data.

Intensity-storm total relationships

We synthesized precipitation intensity and cumulative precipitation relationships to identify generalized storm and site conditions that are likely to cause overland flow and consequently, soil erosion. Thus, we use runoff generation as a direct proxy for soil erosion, which is generally substantiated for gullying processes (e.g. Kirkby and Bracken, 2009). Quantitative runoff-generation analogues for both infiltration-excess overland flow (exceeding the infiltration rate capacity of the soil; e.g. Horton, 1945) and saturation-excess overland flow (i.e. exceeding the storage capacity of the soil; e.g. Dunne and Black, 1970a, 1970b) provide the basis for our methodology. This occurs within a threshold framework inspired by that originally developed for the empirical prediction of shallow landslide initiation (e.g. Caine, 1980, Guzzetti *et al.*, 2008). We note that our approach is nearly identical to that recently developed by Mirus and Loague (2013) who developed a quantitative format of the classic hillslope hydrology diagram by Dunne (1978) and who showed its applicability to a wide range of landscapes and environmental conditions. The purpose of our analysis is to establish an empirical method for identifying landscapes (and archaeological sites) that may be subject to runoff, and potentially soil erosion, from a wide-range of rainfall conditions.

The ratio between rainfall intensity (i) and the near-surface, average field-saturated soil hydrologic conductivity (K) determines which storms are capable of infiltration-excess overland flow. Overland flow and subsequent potential soil erosion will result when this ratio is greater than unity such that water on the surface is unable to infiltrate. Defining $\bar{I}$ as the normalized storm intensity results in:

$$\bar{I} = i/K \tag{1}$$

Field infiltration measurements from both existing reports (Pederson *et al.*, 2003; O'Brien and Pederson, 2009b) and new data collected specifically for this study using a mini-disk infiltrometer provide K values for our analyses (Figure 4, Supporting Information Table S1). We multiplied all field infiltration values by 0.3 to adjust the field data into the Green–Ampt parameter ($K_{G\text{-}A}$), according to previous work in similar environments (e.g. Bouwer, 1966; Grayson *et al.*, 1992; Howes and Abrahams, 2003). The infiltration data were assigned to one of nine mapped substrate categories (Figure 4 plus 'bedrock' and assumed to have zero infiltration capacity) to generate spatially-averaged singular substrate values for each site (Table I). These represent substrate area weighted-average values over each site watershed, thereby indirectly accounting for inherent spatial and geomorphic variability. Whereas ponding and overland flow are not expected to occur everywhere in watersheds, overland flow is often pervasive from upslope contributing areas in semi-arid landscapes, and especially those with expanses of exposed bedrock and/or mantled by coarse colluvium such as found in Grand Canyon (Pederson *et al.*, 2006a; O'Brien and Pederson, 2009b). Thus, the site-averaged values provide a simplified, but still relevant model for the complex processes involving concentrated runoff from impermeable upslope areas onto those with relatively erodible surfaces.

Although the effect of precipitation-induced saturation on landscape change can be analyzed in the time domain (e.g. storm duration relationships, Caine, 1980), this requires making considerable assumptions about the physics of infiltration and associated parameters (e.g. Smith, 2002). Instead, we investigated saturation effects in the volume domain using each storm's cumulative precipitation total, where storm total is the

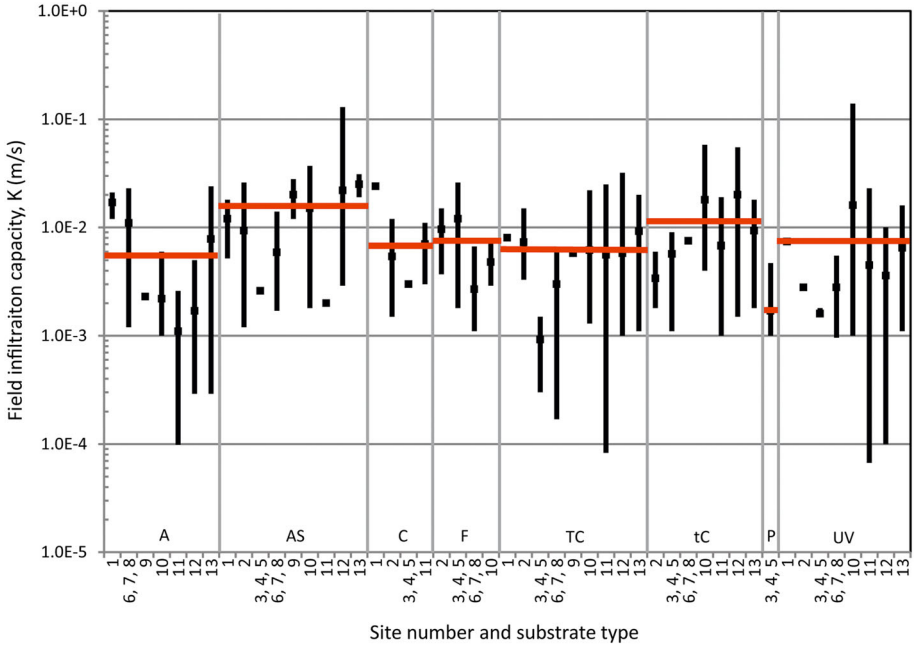

Figure 4. Field soil infiltration (K) data (mean indicated by squares, with vertical bars for maximum and minimum values) at all sites, discretized by substrate category (A = alluvium, AS = aeolian sand, C = colluvium, F = fluvial terrace, TC = thick biological soil crust, tC = thin biological soil crust, P = playa (hardpan evaporative crust over sandy substrate), UV = under vegetation). Horizontal red bars are substrate averages weighted by the number of measurements at each site (see Table S1). Data from Pederson *et al.* (2003), O'Brien and Pederson (2009b), and this study. This figure is available in colour online at wileyonlinelibrary.com/journal/espl

cumulative precipitation of individual storms separated from temporally adjacent storms by at least six hours. This parameter is a proxy for the water available to fill soil pores, especially in arid landscapes where storms are often temporally discontinuous (Kurc and Small, 2004). Whereas subsurface stormflow from up-watershed areas may also contribute to pore filling, its influence is strongest in steep topography (Freeze, 1972; Mirus and Loague, 2013) and where a seepage face can develop (i.e. convex slopes feeding incised channels) (Freeze, 1972). Some of the sites investigated herein meet these requirements (e.g. areas of sites 2, 12, and 13). However, because our methodology is based on simplified metrics that are readily computed from field data for predicting relative overland flow contributions, and because inclusion of subsurface stormflow in our formulation requires more complex three-dimensional analysis, we do not account for subsurface stormflow occurrence explicitly, but do recognize its possible importance for particular cases. In general, its contribution is expected to be minimal in semi-arid environments (e.g. Wainwright, 1994).

To account for antecedent conditions whereby the subsurface does not entirely dry between storms, we calculated the three-day cumulative precipitation of all storms preceding the start of an individual storm. The storm total, S is defined as the sum of the individual storm total (without any subsurface stormflow contribution) and the three-day preceding cumulative total, when applicable. Research from other areas in the desert southwest of the United States with similar overall climate and soil infiltration characteristics (Kurc and Small, 2004) supports the use of a three-day cumulative storm period, showing that precipitation-enhanced soil moisture remains elevated in the subsurface for a few days (with exponential decline time constant of 2.8 days) following infiltration. When S exceeds the subsurface storage capacity (i.e. the *in situ*, available effective soil porosity, θ_e times the effective soil depth, z_e), the soil is considered saturated such that any additional rainfall will generate overland flow on the surface (i.e. saturation-excess overland flow) (Dunne and Black, 1970a, 1970b). Thus, we define $\overline{S}$ as the normalized storm total:

$$\overline{S} = S/z_e\theta_e \tag{2}$$

In the absence of complete site-specific data, we synthesized soil θ_e values for each site (Table I) by subtracting a nominal amount of residual soil moisture (10%) from the dry soil porosity of substrates (Morris and Johnson, 1967) that aligned with our field observations. We calculated z_e as the depth from the average site elevation to bedrock, when known from site observations. For sites located on alluvium or other fine sediments and not immediately underlain by bedrock, we calculated z_e as the depth from the average site elevation to the expected Colorado River elevation at current maximum allowable (dam-controlled) flow. Herein, the maximum flow is taken as 708 m^3/s (i.e. the maximum modified low fluctuating flow condition from Glen Canyon Dam) (Melis, 2011) and is converted to stage elevation by conservatively adding 1.8 m for potential high flows as modeled at the Grand Canyon river gage (a narrow stretch of the canyon, near Phantom Ranch, Figure 1) (Magirl *et al.*, 2008) to the river surface elevation from our LiDAR measurements that were conducted at typical low (140 to 230 m^3/s) flows. Although infiltrating water may flow into the river at the same rate that it is being input to the subsurface and therefore not induce ponding at the archaeological site surface, this depth provides an upper bound on the subsurface storage capacity under reasonable conditions.

We calculated normalized intensity-storm total $\overline{I}$–$\overline{S}$ relationships for all storms at each study site (e.g. Figure 5). In a generalized sense, events with either $\overline{I} > 1$ or $\overline{S} > 1$ indicate that

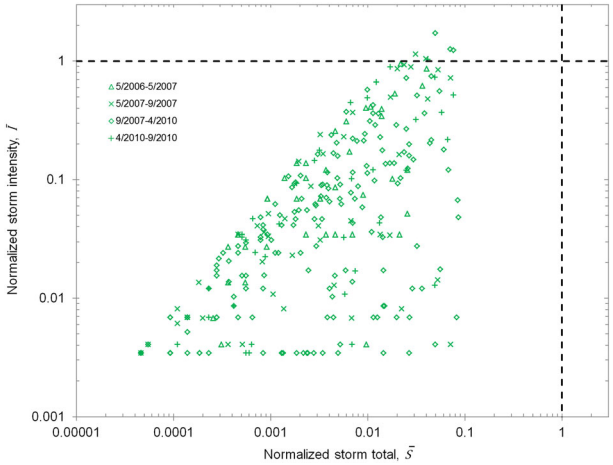

Figure 5. Normalized rainfall intensity-storm total plot for site 5. Idealized runoff thresholds (dashed lines) for infiltration excess overland flow ($\overline{I} > 1$) and saturation excess overland flow ($\overline{S} > 1$) identify storms which may cause gullying and site erosion. At least one storm from each of the latter three time periods plots above the $\overline{I} = 1$ threshold. A single storm for the last time period plots just above the threshold at $\overline{I}$ = 1.03 and a storm for the first time period plots essentially on the threshold at $\overline{I}$ = 0.95. This figure is available in colour online at wileyonlinelibrary.com/journal/espl

overland flow should have occurred. Several features are readily apparent in these relationships, namely, (1) a lower bound exists for $\overline{I}$ based on the minimum measurable 10-minute rainfall intensity (i.e. limited by the programmed rain gage sensor resolution of 0.0254 mm/four-minute interval), (2) an upper bound for $\overline{S}$ exists that is dependent on the (large) effective storage capacity of the subsurface, and (3) a linear increasing relationship is observed between maximum $\overline{I}$ and $\overline{S}$, coincident with an expected increase in rainfall intensity with storm size. In the provided example for site 5 (Figure 5), five storms exceed the infiltration-excess overland flow threshold and likely resulted in runoff, whereas no storms caused saturation-excess overland flow (i.e. no storm exceeded even 10% subsurface saturation). Subsurface stormwater flow should not likely have caused runoff due to the shallow slope (6°) extending over the site and its up-watershed contributing area.

Numerical modeling

The intensity-storm total thresholds provide an indication of which storms are capable of driving site erosion based on an empirical expectation that the highest intensities are responsible for the majority of erosion. To increase our confidence in the threshold results, and as a recommended improvement from previous modeling efforts (Pederson *et al.*, 2006a), we used a numerical rainfall–runoff model (Bedford, 2008) to simulate the dynamics of rainfall, infiltration, runoff, and potential for soil erosion. Our model uses event-based precipitation (i.e. storms) over a site-specific topographic domain and was designed specifically for semi-arid environments. The model (see Appendix for additional information) couples one-dimensional infiltration with two-dimensional overland-flow routing using diffusion wave approximations and mass balance. Thus, the model is distributed and physically-based, accounting for continuity and momentum. Surface water is generated when storage or infiltration capacity are exceeded. Flow (assumed turbulent which is likely during rainfall due to raindrop impacts) is routed across the four cardinal neighbor cells based on their corresponding relative water surface slopes. The diffusion wave method used

here allows water to pond in depressions, which can then be overtopped given sufficient surface water. The design, parameter selection, and verification of the model are discussed by Bedford (2008, who found that resultant flow routing is more sensitive to heterogeneity in fine-scale topographic features than it is to heterogeneity of infiltration values.

To capture the most relevant topographic roughness features in the modeling, we used interpolated 10 to 25 cm resolution terrestrial LiDAR-derived digital elevation model (DEM) grids as base maps (e.g. Figure 3). For each time period, we used the corresponding LiDAR dataset for the beginning of the period (i.e. the May 2006 LiDAR dataset was used for the period from May 2006 to May 2007). In some cases, the site catchment area extended outside the bounds of the terrestrial LiDAR data set; for these, we assimilated available lower resolution (1.5 m) airborne LiDAR data (Davis *et al.*, 2002). Field soil infiltration values (described previously, but here used explicitly rather than as a spatially weighted site average) were assigned to each site and their respective upstream watershed areas based on site-specific geomorphic mapping. For all other model parameters, we used spatially invariant maps with the following values: initial volumetric water content (0.1), saturated volumetric water content (0.25), Darcy–Weisbach friction factor (1), wetting front suction (4 cm), and no interception of rainfall by the vegetation canopy. These values have been found to be robust for simulating high-intensity rainfall over high-resolution topography in other arid and semi-arid environments (e.g. New Mexico, USA; Bedford, 2008). With the exception of a few storms identified in the empirical analysis with low storm totals but high intensity, we limited our analyses to storms with cumulative precipitation greater than 10 mm; these were resampled to one-minute intensity records. We calculated the likelihood for storm-generated runoff in each model through computation of a runoff coefficient (R), defined as the percent of the storm rainfall that is runoff and that exits the model domain.

To assess storm erosion potential, we calculated bed shear stress on a per-pixel basis. For each pixel in the model domain, we calculate the critical shear stress using

$$T_{\text{crit}} = \Theta_{\text{c}}\left(\rho_{\text{g}} - \rho_{\text{w}}\right) g D_{50} \tag{3}$$

(e.g. Kirchner *et al.*, 1990), where T_{crit} is the critical shear stress needed for grain entrainment, Θ_{c} is the critical Shields stress (0.045) (Pederson *et al.*, 2006a), ρ_{g} is the density of the soil (2650 kg/m^3), ρ_{w} is the density of water (1000 kg/m^3), g is the acceleration due to gravity, and D_{50} is the median grain size. The mean D_{50} (as measured by sieve shaker and Coulter laser particle-size analyzer) for 13 samples from two of the sites presented herein is 0.11 mm, indicative of fine to very fine sands (Figure 6). These values represent the fine-grained terraces and aeolian-reworked sediments that form the substrates for many archaeological sites throughout Grand Canyon (Draut *et al.*, 2008). The resultant mean critical shear stress value (0.08 N/m^2) represents a minimum threshold based on sediment transport theory (e.g. García, 2008) as verified by experimental results (e.g. Ahmad *et al.* (2011) obtained T_{crit} = 0.094 N/m^2 for a 0.15 mm diameter pure sand). However, the erodibility of real surfaces is variable due to cohesion and topographic attributes such as grain projection, exposure, and heterogeneities (Kirchner *et al.*, 1990). In addition, the presence of biologic crusts and vegetation at many of the archaeological sites likely increases the critical shear stress needed for entrainment (Prosser and Slade, 1994; Belnap, 2006; Kidron, 2007; Rodríguez-Caballeroa *et al.*, 2012; Sankey and Draut, 2014). Thus, we also utilize a slightly higher critical shear stress threshold (1 N/m^2) for identifying probable site erosion, and show results for both ranges (e.g. Figure 3C).

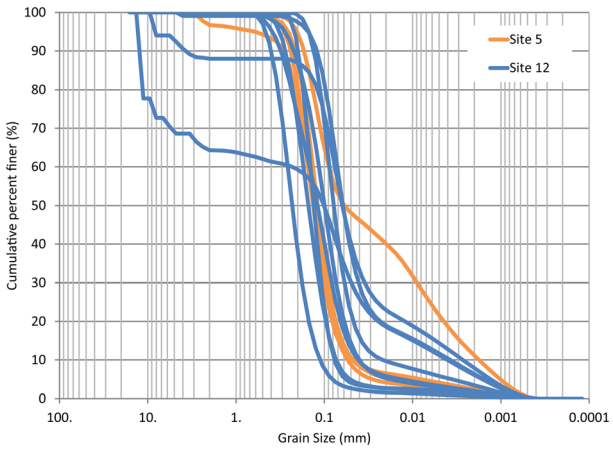

Figure 6. Surficial sediment grain size distribution at two archaeological sites in Grand Canyon. Soils are fine to very fine grained sands with mean D_{50} = 0.11 mm. This figure is available in colour online at wileyonlinelibrary.com/journal/espl

For each storm, at each modeled pixel, we calculate the instantaneous bed shear stress (T_{bed}) based on the maximum flow depth experienced at 60-second intervals (H_{60}) and inserted into the depth–slope product shear stress formula (Julien and Simons, 1985):

$$T_{\text{bed}} = \rho_{\text{w}} g H_{60} G \tag{4}$$

where G is the topographic slope (gradient). Locations likely to experience overland flow capable of causing erosion are those with bed shear stress above the critical threshold. The result is a site response for expected overall erosion from individual storms (e.g. Figures 3C and 3D). We note that due to the inherent generalities made in our formulation (e.g. spatially homogenous critical bed shear strength, of which site specific data is not available), the model results are not intended to identify specific areas of erosion. Rather, they are meant to identify whether runoff and consequent erosion are likely to occur at a particular site from a given storm.

Results

Site change and active geomorphic processes

As should be expected for such a spatially complex study area as Grand Canyon, our LiDAR-based change detection results vary considerably between sites (Figure 1). Whereas some sites underwent topographic change resulting from aeolian deposition and erosion, others eroded from concentrated runoff and gullying, and at some sites, both processes occurred. Most sites exhibited some measurable change, but in some cases, no changes were detected. Despite these variations, the change detection data support several general observations.

We measured a total of nearly 1500 m^2 of site area (9% of the total area surveyed at all sites) that underwent significant landscape change (i.e. greater than our change detection thresholds) over a 4.4-year period. We note that this magnitude partially represents areas that underwent multiple episodes of change (i.e. deposition followed by erosion or vice versa). Our monitoring results indicate a net erosional signal throughout the study sites (Figure 1) with overall erosional area from all processes (962 m^2) outpacing deposition (497 m^2) by nearly 2:1. Likewise, erosional volumes (185 m^3) also outpaced those from deposition (72 m^3; Supporting Information Table S2). Of the 13 sites we monitored, nine by area (69%) and eight by volume (62%)

had erosion totals greater than that caused by deposition. During only one monitoring time period (May 2006–May 2007) did the total area and volume of deposition (318 m^2 and 48.6 m^3) exceed that from erosion (28 m^2 and 2.7 m^3; Figure 1, Table S2). The strongest process signal by volume is runoff-induced erosion (135 m^3) which is nearly double that from all deposition processes (6 m^3 from runoff and 66 m^3 from aeolian processes). This indicates that far more sediment was transported away from the archaeological sites than to them.

Our measurements can be used to obtain a short-term (4.4 years) estimate of the sediment transport rate from the inner Grand Canyon landscape (i.e. that located at the canyon bottom and composed of recent Holocene deposits) by summing the erosion measured from all our surveyed sites. Using the combined net (erosion – deposition) volumes of sediment transported at all of the sites (113 m^3), assuming an *in situ* soil density of 1200 kg/m^3 (Webb *et al.*, 2000), and dividing by the entire areal component of this study (16 500 m^2) yields a surface erosion rate of 18.7 Mg/ha/yr. (1.6 mm/yr). Because some periods of change at the sites occurred over time intervals shorter than 4.4 years, this calculation provides a lower bound estimate. Our erosion rate is two to five times higher than those measured in other soil-mantled semi-arid areas of Arizona (7.6 Mg/ha/yr. by Zhang *et al.*, 2011; 3.8 Mg/ha/yr. by Ritchie *et al.*, 2005) and an order of magnitude greater than long-term bedrock-based rates measured in Grand Canyon (2.3 Mg/ha/yr. by Webb *et al.*, 2000; 1.7 Mg/ha/yr. by Pederson *et al.*, 2006b). The higher erosion rates from the soil-mantle-based areas compared to the bedrock-based areas are expected by simple virtue of differences in material strength. The lower rates of all but the Zhang *et al.* (2011) case (based on a two-year measurement) should also be expected given that these studies looked at longer time intervals (~10 years for Webb *et al.* (2000) using empirical regression methods on tributaries, ~30 years for Ritchie *et al.* (2005) using cesium-137 (^{137}Cs) dating, and hundreds of thousands of years for Pederson *et al.* (2006b) using a combination of optically stimulated luminescence, uranium series, and cosmogenic dating techniques). Thus, coincident with the findings of Gardner *et al.* (1987), we find that the transport rate is dependent on the interval over which it is calculated. We explain the lower Zhang *et al.* (2011) rate by noting that the sites contributing to our erosion rate were selected specifically because erosion was expected to occur there. In general, we find that our measurements provide a robust estimate of short-term erosion rates affecting many river-level landscapes in Grand Canyon.

Although the spatial distribution of the sites is uneven throughout the river corridor, the data do not support any systematic increase or decrease in overall sediment transport rates moving downstream. Nor are overall runoff processes (erosion + deposition) more or less active with respect to distance from the dam at the upstream end of Grand Canyon. Rather, topographic changes are largest specifically where active aeolian environments exist; these are located throughout the canyon (e.g. sites 1, 2, 9, and 12). In addition to being subjected to aeolian processes, many of these active sand areas are also subject to concentrated gullying (Figure 1) – this interplay of processes is key to understanding the cyclic change to which sites are subjected.

Precipitation thresholds

The normalized $\bar{I}$–$\bar{S}$ precipitation threshold for erosion provides a unifying approach to incorporating the spatial, temporal, geomorphic, and meteorological characteristics of landscapes affected by overland flow. We believe that this approach moves empirically-based landscape change analysis forward from those based solely on meteorological conditions (e.g. those using only precipitation totals) to that based on geomorphological setting and the physical processes of infiltration. Used over the length of a substantially-long semi-arid fluvial landscape, it synthesizes likely agents of runoff and soil erosion over a wide range of substrates and morphologies.

Plotting the $\bar{I}$–$\bar{S}$ relationship for all storms at all sites indicates that the overall response is governed by infiltration-excess flow and that $\bar{I}$ scales with $\bar{S}$. All storms (e.g. Figure 5 at site 5) plot well below (i.e. $\bar{S} < 0.2$) any reasonable threshold limit (i.e. $\bar{S} = 1$) for saturation-excess overland flow. As noted previously, this is expected given the large storage capacity (depth and porosity) of site substrates; in the absence of heterogeneous perched zones, saturation-excess overland flow is not expected at typical sediment-based archaeological sites from storms occurring in Grand Canyon or other similar semi-arid and arid environments (Howes and Abrahams, 2003; Tucker *et al.*, 2006). To compare the site to site response, we therefore show only the single highest normalized intensity ($\bar{I}_{max}$) storm for each site and monitoring period (32 data points; Figure 7).

The empirically-based threshold results correctly predict 66% of the storm responses associated with either documented soil erosion (i.e. green symbols with $\bar{I} > 1.0$ in Figure 7) or a lack of soil erosion (i.e. purple symbols with $\bar{I} < 1.0$ in Figure 7). However, direct interpretation at this simplified level does not sufficiently explain the overall response due to the dependence on average substrate values (K, θ_e) in deriving values of $\bar{I}$ and $\bar{S}$. Variations in K in Equation (1), for example as a result of using minimum values of the hydraulic conductivity at a site, can increase values of $\bar{I}$ for many storms so that they too are greater than 1.0. Thus, we direct the interpretive focus on the fact that storms with documented precipitation-induced erosion (green symbols; Figure 7) have greater $\bar{I}$ compared to those with no documented erosion (purple symbols, Figure 7). Their respective means ($\mu = 1.1$ for erosion and $\mu = 0.7$ for lack of erosion) are statistically different as verified by a t-test ($P = 0.01$). Although this difference could be due to the occurrence of higher intensity storms at sites with documented erosion, we know this not to be true – the storm intensity means ($\mu = 64$ mm/h for storms causing erosion and $\mu = 58$ mm/h for storms not causing erosion) are

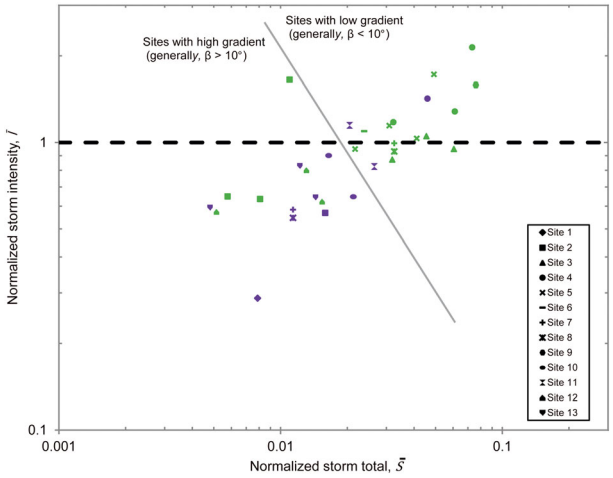

Figure 7. Intensity-storm total threshold plot for the highest intensity storm occurring at each archaeological site during each monitoring period. Green data points are those with documented site erosion resulting from precipitation runoff. Purple data points are those with no documented runoff generated site erosion. Dashed line identifies the normalized intensity threshold at $\bar{I} = 1$. Most sites with steep slope (generally >10°) plot down and to the left of the solid diagonal line (i.e. having both low $\bar{I}$ and $\bar{S}$). This figure is available in colour online at wileyonlinelibrary.com/journal/espl

statistically similar (*t*-test $P = 0.57$), and we have observed high-intensity storms in all parts of Grand Canyon.

Whereas some inconsistency in the results is expected given that rainfall conditions are being linked to soil erosion without inclusion of an implicit soil entrainment mechanism, the grouping of false negatives (data points below the threshold but with documented erosion; sites 2 and 12) are notable. Analysis of the overall topographic slope (β, Table I) at each site provides a plausible explanation; storm responses with low $\overline{I}$ and $\overline{S}$, with the exception of only a few cases (e.g. sites 1 and 9), generally occurred at sites with slopes in excess of 10° (i.e. left of the diagonal line shown in Figure 7). This contrasts with the majority of those that plot above and to the right of this line where average slopes are on the order of 5°. These results are in close alignment with those found by Mirus and League (2013 who found that steeper slopes in their simulations also had low $\overline{I}$ and $\overline{S}$, and were more prone to subsurface stormflow. Our observations of piping conduits in the sidewalls of incised gullies at the steeper sites suggest that this form of flow may be a contributor to overland-flow-induced erosion in some cases.

False positives (data points above the threshold but with no documented erosion) are associated with sites having very low (<1° to 5°) topographic slope (sites 4 and 11). We presume that for these cases, bed shear stresses are sufficiently low to limit the amount of surface erosion even under sometimes intense storm conditions. False positives could also arise when erosion did occur but where our analyses did not detect the change (i.e. below the 3 to 8 cm change detection threshold).

Overall, the results demonstrate the utility of an empirically-based methodology for identifying the major causal factors for runoff and the subsequent erosional response over a wide range of geomorphologic and environmental conditions. Additionally, analysis of false negatives and false positives allow interrogation of other potential factors that may define the generalized response (here, we identified topographic slope, but others factors might also be applicable depending on field settings). These findings could be used to define additional empirical parameters for landscape response (for example, by including topographic slope implicitly in the threshold equations). We note however, that the benefits of a simple model are soon made irrelevant with increasing complexity brought on by including too many additional parameters. In the far end of the spectrum, this methodology becomes that implemented in a numerical model, one of which we present in the following section.

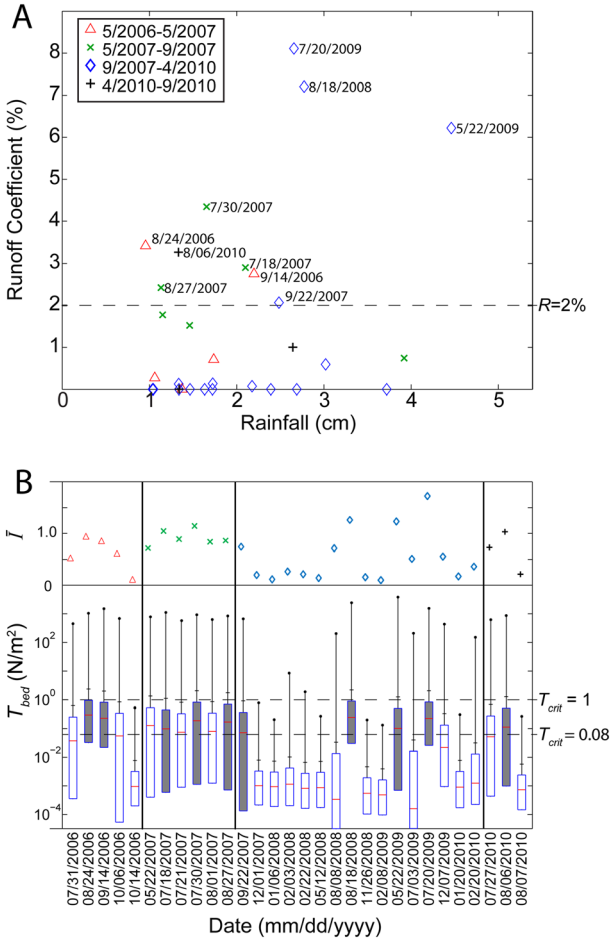

Figure 8. (A) Predicted runoff coefficient (volume of runoff/surface area) and (B) $\overline{I}$ and bed shear stress for all modeled grid cells for each storm at site 5. For the boxplots in (B), the central boxes denote inner quartiles, the central line denotes the median value, whiskers are at one standard deviation, and dot symbols are maximum values. Storms with runoff coefficient > 2% in (A) are shaded in (B). Medians of all shaded storms exceed the theoretical critical shear stress threshold ($T_{crit} = 0.08$, lower dashed horizontal line). Generally, standard deviations exceed the $T_{crit} = 1$ threshold (upper dashed horizontal line) only for the shaded (high runoff) storms. Overall, storms with high $\overline{I}$ coincide with those predicted to have high runoff and high bed shear stress, thereby indicating increased potential for site erosion. This figure is available in colour online at wileyonlinelibrary.com/journal/espl

Verification with rainfall–runoff model results

We present numerical modeling results from a site (site 5) in eastern Grand Canyon as verification for the empirical threshold results and also to demonstrate the interplay between rainfall, runoff, and erosion at the site scale. Modeling performed for several other sites as a part of this study reinforces these points.

At site 5 (Figures 2A and 3), we simulated the runoff response from 30 measured storms between May 2006 and September 2010. Storm totals exceeded 10 mm for all events with the exception of a high intensity, low (8.4 mm) storm total on August 24, 2006. The model predicted appreciable runoff (runoff coefficient, $R > 2\%$) for 10 events (Figure 8A) including the highest intensity event identified for each time period by the empirical intensity-storm total results (Table III). Median bed shear stresses were above critical entrainment ($T_{bed} > T_{crit}$; Equation (3)) for most storms (Figure 8B) and over significant parts of the model domain for storms with $\overline{I} > 1.0$ (Figure 3C). Storms with $\overline{I} < 1.0$ showed only limited bed shear response (Figure 3D) and generally occurred during the winter (November through February).

Areas of measured erosion from a runoff source (i.e. those in contact with a gully flow line as shown in Figure 3B) are generally captured by the spatial distribution of large runoff depths and consequent high bed shear stresses (Figure 3C). Areas with high infiltration capacity, for example fluvial terraces (Figure 4), coinciding with the left side of Figure 3A, did not result in high bed shear stresses, except at concentrated areas in gullies (e.g. only gully bottoms within the fluvial terrace areas on the left side of Figure 3C). Areas without good correspondence between measured topographic change and high bed shear may be from either the magnitude of erosion being below the change detection threshold (for this example, 5 cm), or potentially from incremental topographic changes occurring during the storm (i.e. headward propagation of a knickpoint or sidewall bank collapse – see Figure 3B) that are not captured by the model. At this spatial and parametric resolution, the power of the model lies not in its prediction of the exact location of expected erosion, but rather in confirming the empirical threshold results (Figure 7) and identifying the expectation (or not) that erosion will occur from different types of storms.

Predicted return period for storms

Our generalized storm intensity-storm total threshold and site-specific interpretations provide quantitative linkages between intense storms and semi-arid site erosion. Correlated erosion-inducing storm intensities were substantial, with 10-minute intensities averaging 64 mm/h (Table III) and with 67% of these storms having intensities greater than 50 mm/h. The question therefore arises whether the erosion-inducing storms were exceptional when compared to previous observations in Grand Canyon. Precipitation results from a 2002 study conducted on river corridor archaeological sites (Pederson *et al.*, 2006a) indicate that widespread gully erosion occurred from storms of the same order of magnitude as those identified here. In 2002, maximum (35-minute) storm intensities reached 79 mm/h and storm totals reached 46 mm (with corresponding $\overline{I} > 1.0$ and $\overline{S} < 0.2$ using identical site parameters presented herein), thereby substantiating our generalized $\overline{I}$ versus $\overline{S}$ threshold methodology. Unfortunately, there are no long-term (30+ year) high frequency (sub-10-minute interval) records available with which to determine recurrence intervals for storm-intensity. Instead, we investigate the corresponding cumulative daily, seasonal, and annual precipitation totals for correlated erosion-inducing storms by comparing our data to that from two nearby long-term (75+ year) rain gages located roughly at Colorado River level (Lees Ferry and Phantom Ranch, Figure 1).

On a daily basis, the precipitation totals corresponding with site erosion-inducing events are not uncommon. Recurrence intervals for erosion-inducing storms (green symbols in Figure 7) range between 0.1 and 13.8 years (Table III), and the majority occur with less than two-year periodicity at Lees Ferry (58% of storms) and Phantom Ranch (83% of storms). All recurrence intervals greater than five years are from the Lees Ferry gage, which is located farther from most of the sites investigated herein (Table III, Figure 1). Thus, we judge that lower recurrence intervals from Phantom Ranch are more representative for our data comparison. Analysis of daily storm total recurrence intervals calculated from the long-term records for the time period before completion of Glen Canyon Dam (i.e. prior to January 2, 1963) compared to that following completion of the dam indicates that the number of potentially erosion-inducing storms has not changed substantially over time. The average difference in recurrence intervals (pre-1963 minus post-1963) is less than one year (ranging from −0.8 to 0.1 years) using the Phantom Ranch data and less than three years using the Lees Ferry data. Thus, we infer that post-dam changes to the landscape cannot be linked to differences in short-term climate before versus after dam construction.

Examination of annual precipitation data from the two weather station sites supports the notion that the documented erosion was not associated with above average rainfall conditions. Although recent analyses of long-term regional precipitation data (Hereford *et al.*, 2014) indicate that multidecadal episodes of wet conditions can initiate terrace and consequent site erosion, our data indicate that erosion can also occur within periods of extended drought (i.e. the early twenty-first century drought in which this study was conducted; Hereford *et al.*, 2014). The average annual precipitation during our monitoring period (2006–2010) at Phantom Ranch (228 mm) and Lees Ferry (112 mm) were nearly identical or slightly lower than their respective long-term averages (231 mm and 148 mm). Similarly, evaluation of seasonal precipitation totals only provides weak support that above average conditions could have been responsible for site erosion. In a study conducted in eastern Grand Canyon near sites 3 and 8 (Figure 1), Hereford *et al.* (1993) found that arroyo (gully) downcutting and erosion coincided with seasons (therein defined as that occurring during either the 'cold season' between November 1 and February 28 or the 'warm season' between June 15 and October 15) with above average precipitation (i.e. referenced to the 1990 warm season with 120 mm of precipitation and which caused definitive erosion). For five seasons between 1966 and 1990 (Table IV) that coincided with runoff, debris flow activity, and probable erosion of river terraces (Hereford *et al.*, 1993), the average seasonal precipitation was 134 mm.

During our study period, the average seasonal precipitation coinciding with erosive events in which seasonal data are available (warm season 2006, 2007, 2009, 2010) was 110 mm. Cumulative precipitation for only two of these (warm seasons 2006 and 2010) coinciding with 5 of 12 storms (Tables III and IV) were above or near the threshold (>120 mm) defined by Hereford *et al.* (1993). Four other erosion-inducing storms occurred during warm seasons with below average precipitation, two occurred outside of either cold or warm season, and one has incomplete seasonal data available. The lack of erosion-inducing cold season storms, despite cumulative precipitation exceeding previously established erosion thresholds, is corroborated by our modeling results; for example, the results for site 5 (Figure 8B) indicate that median bed shear stresses never exceeded that required for erosion (i.e. T_{crit}) during any cool season event (e.g. Figure 3D). One of the below average warm season events causing erosion (July 20, 2009 at sites 3 and 5) had a respectable 76 mm/h storm intensity, but coincides with a seasonal precipitation of only 32 mm. This single storm accounted for 84% of the seasonal precipitation, highlighting the importance of single strong storms on morphological change.

Table IV. Seasonal cumulative precipitation causing runoff-induced site erosion during the period 1966–1990, according to Hereford *et al.* (1993) and during the present study (2006–2010).[a]

Season (bracketing dates)	Seasonal cumulative precipitation at Phantom Ranch (mm)
1966–1967 cold season (November 15, 1966–January 15, 1967)	53
1972 fall season (September 15, 1972–November 15, 1972)	114
1978–1979 cold season (November 1, 1978–February 28, 1979)	248
1983 warm season (June 15, 1983 –October 15, 1983)	135
1990 warm season (June 15, 1990 –October 15, 1990)	120
2006 warm season (June 15, 2006 –October 15, 2006)	210
2006–2007 cold season (November 1, 2006–February 28, 2007)	22
2007 warm season (June 15, 2007 –October 15, 2007)	78
2007–2008 cold season (November 1, 2007–February 28, 2008)	193
2008 warm season (June 15, 2008 –October 15, 2008)	(25)[b]
2008–2009 cold season (November 1, 2008–February 28, 2009)	82
2009 warm season (June 15, 2009 –October 15, 2009)	32
2009–2010 cold season (November 1, 2009–February 28, 2010)	144
2010 warm season (June 15, 2010 –October 15, 2010)	118

[a]Three storms occurring outside the defined warm and cool seasons (see Table III) are not used in this analysis.
[b]Data is incomplete (missing 71% of records) and not used for analysis.

Thus, although some of our data corroborates that above average seasonal precipitation conditions are responsible for site erosion, particularly during summer monsoon conditions, there is more support for the hypothesis that individual high-intensity storms are the principal driving factor, and such monsoonal storms are likely common in Grand Canyon with respect to overall daily, seasonal, and annual climatology. Erosion-causing events with similar recurrence interval (3–5 years) as that identified in our analyses have also been documented in the semi-arid high plains of Colorado (Tucker *et al.*, 2006) indicating that storm-induced gullying is both a widespread and common phenomenon in the southwestern United States. Our analyses therefore suggest that the best predictor of site erosion in semi-arid landscapes is related to short-term (10-minute) storm intensity rather than storm totals or cumulative seasonal totals; short time-frame storm intensities have also been shown to be applicable for post-fire debris flow prediction (Kean *et al.*, 2012). The data do support that erosion is typically linked to warm season, highly convective desert monsoon storms, but also indicates that erosion can occur outside of wet years, or even wet seasons. These are key points to consider when considering weather and climatology in all dryland landscapes.

Combined Site Response from Fluvial–Aeolian–Alluvial Interactions

The storm intensity threshold results, their seasonality, and their verification with numerical-model-based runoff-erosion analyses provide a springboard for explaining why semi-arid landscapes respond in different ways to short-term meteorological events, and when applicable, potentially to fluvial forcing via upstream dam operations. For example, in regions with an upwind aeolian sediment supply, such as might form from fluvial sandbar creation, we might expect adjacent alluvial gullying to be at least partially offset by aeolian deposition (Draut and Rubin, 2008; Sankey and Draut, 2014). However, in aeolian-sediment-starved regions, we might expect that storms will cause cumulatively increasing erosion without any possibility of gully annealing. Knowing what singular possibilities can occur in a dryland landscape such as Grand Canyon can help to inform how similar landscapes may respond and evolve.

We highlight three possible outcomes (erosion resulting from no upwind sand supply, erosion despite an upwind sand supply, and erosion prevented by an upwind sand supply) from our change detection results as examples of future expected geomorphologic scenarios in a fluvial–aeolian–alluvial system. Other scenarios obviously exist, but these three provide information on highly plausible situations in similar dryland landscapes as those studied herein. The study sites portray a spectrum of responses, from cumulative gully erosion to partial gully infilling, and the monitored time period brackets a single HFE conducted during March 6–8, 2008 (consisting of a 60-hour 1210 m^3/s water release from Glen Canyon Dam; Melis, 2011) allowing us to test whether fluvial deposited sediment affected the sites.

Precipitation-induced erosion without upwind aeolian sand supply

Where modern upwind aeolian sediment supply is lacking, a negative (erosional) effect is expected with respect to landscape evolution. Our observations from site 5 with three traversing gullies (Figure 2A; Table V) confirm this expectation and document continuing degradation from episodic gullying without significant aeolian infilling. Beginning in May 2006, we documented both progressive gully erosion and episodic deposition over time (Figure 3). Between May 2006 and May 2007, the central part of the site underwent deposition along a length of 1.8 m. By September 2007, an additional 1.5 m of this gully area showed evidence of runoff-induced infilling. The deposition can be linked to temporary stability offered by recent attempts at erosion control via wood and rock check dams in the lower part of the site (O'Brien and Pederson, 2009b). During both time intervals, our observations and interpretations suggest that overland-flow-induced gullying occurred in the upper part of the site, but was less than the LiDAR change detection threshold.

Over the next 2.5 years (up to April 2010), all three gullies underwent erosion, with the southern, initially very shallow (<3 cm) gully downcutting by an average of 6 cm. Continued downcutting of 4 cm occurred in this (southern) gully during the 2010 summer monsoon. For each time period, at least one storm either exceeded or came close to exceeding (0.95) the $\bar{I} = 1$ threshold (Figure 5), implicitly linking intense storms with overland-flow-induced erosion. During the entire monitoring period, only minimal aeolian deposition (averaging 5 cm and totaling 0.2 m^3) occurred throughout the site and was concentrated adjacent to, but out of, the southern gully. Whereas a few isolated patches of active aeolian sand occur adjacent to the site, large sand deposits or fluvial sand bars without biological soil crusts or dense vegetation are not situated in upwind positions to provide sand for aeolian gully infilling. In addition, no new upwind deposits of sand were formed

Table V. Site descriptions for select archaeological sites in Grand Canyon.[a]

Site #	General description	Archaeological time period	Geomorphological description	Number of traversing gullies
2	Habitation areas with probable buried structures	1050 to 1150 CE	Debris fan covered with fluvial, colluvial, and dune sediment	3
5	Occupation area with artifacts and fire-cracked rocks	1050 to 1150 CE	Low angle terrace riser adjacent to area of fluvial and playa sediments	3
9	Overhanging sandstone ledges used as prehistoric shelters with pottery sherds, lithic debris and fire cracked rocks	1000 to 1150 CE	Sand ramp leading to sandstone ledges	2
12	Habitation area with agave roasting pits and artifacts	900 to 1050 CE and 1200 to 1800 CE	Fluvial terrace at distal end of debris fan capped by dune sand	3

[a]See Collins *et al.* (2009, 2012) for additional details.
[b]CE = common era.

here during the 2008 HFE (Draut *et al.*, 2010a). Our results therefore provide supporting evidence for the hypothesis of Draut (2012) that areas without modern upwind fluvial sand deposits (i.e. RFS sites) will have less active aeolian dune fields and will be less capable of counteracting gully erosion. Without extremely large floods that could build sand bars in upwind locations (e.g. a 4800 m^3/s flood) (Magirl *et al.*, 2008), we expect that the existing gully systems at this and similar sites will continue to incise with potential loss of artifacts and the depositional context in which they originally existed.

Precipitation-induced erosion with upwind aeolian sand supply

For landscapes located in proximity to modern upwind fluvial-sourced aeolian deposits, restorative gully infilling feedback is expected, but will be countered by the magnitude of precipitation-induced erosion. At sites 9 and 12, we documented large-scale (>50 cm downcutting) gully erosion partially offset by aeolian infilling. At site 9 (see description in Table V), our observations of two gullies document a cyclical pattern of runoff-induced erosion, followed by topographic lowering adjacent to the gully margins and aeolian infilling. In late summer 2007, one gully formed as a result of significant runoff with substantial (>50 cm) downcutting and erosion, but by September 2007, aeolian sediments had begun to infill the gully. Between September 2007 and September 2010, additional gullying and erosion up to 160 cm in depth occurred, most likely coincident with a storm that well-exceeded (1.6) the $\bar{I}$ = 1.0 threshold (Figure 7). However, by the end of this period, gully wall slumping and aeolian infilling up to 60 cm deep began to smooth the gully cross-section. It is not possible to quantitatively discretize the depositional component caused by each of these processes, but we know from on-site inspection that aeolian infilling can be substantial (tens of centimeters). Partially vegetated sand dunes up to 10 m in height are located immediately upwind of the site providing a source for aeolian-transportable sand. These dunes, in turn, are restored by nearby fluvial sand bars; this is therefore a MFS site as defined by Draut (2012). During the 2008 HFE, upwind sand bars grew in both area and volume, and remained enlarged through the 2008 spring windy season (Hazel *et al.*, 2010). Thus, although this site suffered overall erosion during our study, it shows potential for aeolian infilling.

At site 12 (Figure 2B, Table V), some 160 river kilometers downstream from site 9 (Figure 1), we documented a similar history of cyclical erosion and infilling, but here, both fluvial and terrestrial sand supplies are more limited than at site 9. Between May 2006 and September 2010, we documented isolated (<15 cm) erosion within two gullies. In a third gully (Figure 2B), we observed cyclic large-scale gullying and infilling from aeolian dune deposits located immediately adjacent to the area. Gullying occurred to an average depth of 18 cm between May 2006 and May 2007, to an average depth of 25 cm (and maximum of 50 cm) between May 2007 and September 2007, and then to an additional average depth of 20 cm between September 2007 and September 2010. Despite low values of $\bar{I}$ (0.6 to 0.8) during these periods, our modeling results indicate that critical bed shear stresses were exceeded at specific areas (i.e. gullies) within the domain for many storms during these periods. This highlights the limitations of using site average values for interpreting specific areas of erosional response, but also suggests that both subsurface stormwater and infiltration-excess overland flow may be occurring here.

Between September 2007 and September 2010, some erosion at the third gully was offset by a similar magnitude of infilling from both overland flow/backwasting and aeolian sources. This gully therefore became wider over the course of the five-year time period, with somewhat muted vertical incision. Despite the presence of an on-site aeolian sand supply, modern fluvial sand deposits are currently generally small (approximately a few hundred square meters) upwind of the site. An HFE sand deposit with a favorable upwind location to the site was reported to have formed in 2008 (Draut *et al.*, 2009b) but its longevity was on the order of several months, being quickly eroded by daily dam-regulated fluctuations of the river (Draut *et al.*, 2010a). However, archived aerial photographs taken shortly after high flows in the mid-1980s and 1996 show a large amount of fluvial sediment adjacent to and upwind of this site, indicating that a larger aeolian sand supply had been available earlier in the post-dam era (i.e. it is an MFS site). There is therefore some potential here for periodic aeolian infilling of gullies.

Precipitation-induced erosion prevented by aeolian sand infilling

If nearby aeolian deposits are upwind, and infilling is of sufficient magnitude, net gully erosion may be prevented altogether as a landscape response. Our observations from site 2 (see description in Table V) provide confirming evidence of this process. Between May 2006 and May 2007, a 260 m^2 aeolian sand deposit formed to an average depth of 20 cm, burying a majority of the central gully at the site. Wind direction and wind speed during this time were favorable for aeolian transport from a nearby sandbar and dune deposit (Draut *et al.*, 2009a), and we witnessed aeolian transport via this mechanism here during this study. Over the same time period, runoff-generated erosion occurred at two other (lateral) gullies (albeit from storms somewhat below (0.6) $\bar{I}$ = 1.0, Figure 7; see previous discussion concerning the steep slope at this site), suggesting that the aeolian deposition prevented erosion in the central gully. Additional erosion occurred in one of the lateral gullies over the next four months (up until September 2007), and whereas aeolian erosion of the previous deposit also occurred, no precipitation-induced erosion in the central gully was observed. This again suggests that the aeolian deposit had a mitigating effect against gullying. Over the next three years (September 2007 to September 2010) only minor aeolian erosion, overland flow, and hillslope creep processes affected the site. Interestingly, the 2008 HFE had little beneficial influence to the site. Although sand bar volume increased upwind of the site, sand bar area decreased, thereby limiting the potential for new aeolian sand transport (Draut *et al.*, 2010a).

Discussion

The presented results, along with our interpretations of individual site response, provide important insights on coupled fluvial–aeolian environments subjected to periodic overland flow erosion. In addition to having important management implications, they also speak to the wider subject of landscape evolution.

First, we find that short-term erosion rates in Grand Canyon, as is the case in many semi-arid landscapes, can be particularly high and are caused by short-term high-intensity rainfall events exacerbating gully erosion. However, we also find that aeolian deposition can mitigate erosion in some cases. At four of our

monitored sites (sites 2, 9, 10, and 12), gullies were either partially infilled or were prevented from further net downslope development due to aeolian deposition (Figure 1; see also Collins *et al.*, 2009, 2012). This is an indication that sites are still subject to the same aeolian processes that have occurred in the Grand Canyon since the archaeological sites were first buried some one thousand years ago by fluvial and aeolian sediments (e.g. Draut *et al.*, 2008). Despite this promise for archaeological site preservation, our observations show that gully annealing can only occur under a specific set of conditions related to fluvial sand availability and wind transport direction. This confirms earlier findings (e.g. Draut and Rubin, 2008; Draut, 2012; Sankey and Draut, 2014) that aeolian sand transport (and thus gully annealing) is more common and of greater magnitude at sites in MFS sand deposits (those downwind of current, post-dam fluvial sandbars) than in RFS sand deposits (i.e. those only downwind of sand deposits formed from large, pre-dam floods). For example, in Grand Canyon, site 2 is located downwind from a modern-fluvial-sourced sand deposit and underwent significant aeolian deposition compared to a nearby site with similar wind conditions (site 5) but lacking a modern-fluvial-sourced aeolian sand supply (Draut and Rubin, 2008).

Second, we find that anthropogenic actions (i.e. high flow dam releases to build downstream sand bars) are dependent on a narrow set of conditions for successful coupling of fluvial deposition and aeolian sand transport. Although we recorded aeolian sand deposition at several MFS landscapes during a monitoring period that included a HFE in 2008, we found little indication of long-term sand deposition beyond the edge of the river. Sand bars along the river did increase in both area and volume following the high flow release (Hazel *et al.*, 2010), providing a potential aeolian sand source for aeolian transport. However, the majority of aeolian deposition identified during our study (2006–2010) occurred prior to 2008 and no systematic increase in deposition after the high flows can be discerned from the data (Figure 1). With the exception of site 6 (see succeeding discussion), wind transport conditions over the year following the HFE were generally not favorable (i.e. unfavorable wind direction, presence of topographic and vegetative barriers) for aeolian transport from the newly built sand bars to many of the sites (Draut *et al.*, 2010a). Rather, most of the new depositional areas were caused by reworking of existing on-site aeolian dunes (Collins *et al.*, 2012).

Despite the lack of clear correspondence between attempts at anthropogenic sand bar building and a decrease in nearby landscape erosion, one site (site 6) provides a good case study of the long-term potential effects from a high flow release in that it is located in an active aeolian dune setting immediately downwind of a fluvial sand bar (see Collins *et al.*, 2012). Although the sand bar here was significantly eroded by flow fluctuations soon after the high flows, substantial aeolian sand was also transported inland by wind during this period (Draut *et al.*, 2010a) and over the next several years (Draut, 2012). Cross-section surveys of the bar-dune system over a six-year time period following the 2008 HFE, and which spans a time period that includes two additional high flow releases in 2012 and 2013, indicate that the centroid of the sand deposit (as measured individually at the bar and dune deposit) moved inland over 30 m (Draut, 2012; J. Hazel, personal communication 30 May 2014) albeit at an exponentially decreasing rate (Figure 9). This analysis indicates that we should not expect an instantaneous landscape response from anthropogenic high flow releases but rather a lag time of several years or more may be needed to transport sand to adjacent dryland areas.

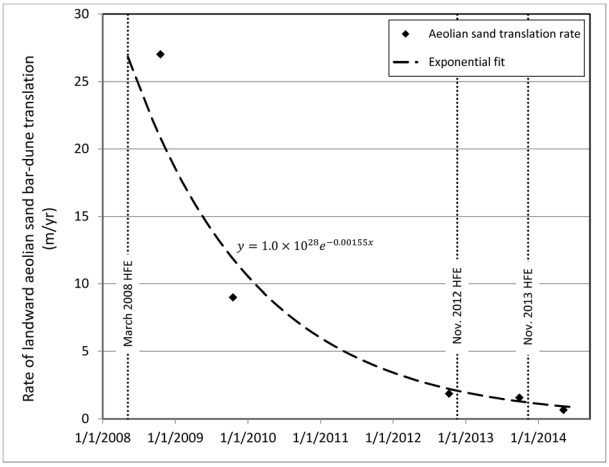

Figure 9. Landward transport rate of fluvial sand bar and subsequent aeolian dune centroid at site 6 following the 2008 high-flow experimental release (HFE). HFEs in 2012 and 2013 added ancillary dunes to the main sand body but do not appear to have affected the overall dune translation rate. Data from Draut (2012) and subsequent unpublished measurements by J. Hazel (Northern Arizona University, Flagstaff, AZ).

Conclusions

Dryland landscapes located near fluvial systems are subject to complex interactions caused by alluvial, fluvial, and aeolian processes with erosion and land degradation most often playing the dominant role (Ravi *et al.*, 2010). Anthropogenic attempts to mitigate erosion, for example, by dam-controlled fluvial sand bar formation and subsequent aeolian deposition, require a detailed understanding of the background landscape response. Our studies of these processes at archaeological sites in a semi-arid landscape provide new insights into predicting future process potential. Construction of a simplified metric capable of identifying the type of overland flow mechanism (i.e. infiltration-excess or saturation-excess) causing erosion identified that infiltration-excess runoff dominates and that short-term (e.g. 10-minute) rainfall intensity is the major driver of gully-induced erosion. These conclusions are likely applicable to a wide-range of dryland landscapes in which somewhat deep, permeable soils are the norm. However, the results indicate that soil surface properties (e.g. infiltration capacity) are critical in determining the hydrologic and geomorphic response of these landscapes, as defined by the normalized rainfall intensity, $\bar{I}$ (see Methods section). More in-depth spatio-temporal prediction of site response can be achieved using numerical rainfall–runoff models with high resolution topographic data as presented herein, but with a coincidental significant increase in model complexity.

Examination of false-positives and false-negatives from the runoff-erosion empirical analysis identified topographic slope as the next most important factor (after $\bar{I}$) for predicting site response. Long-term climate patterns were found to be less important – erosion can be expected in dryland areas regardless of drought conditions as long as storm rainfall intensity is high. These findings may be helpful for future studies, but less so for reconstructing past landscape change estimates where high-resolution precipitation records are not available.

Despite the calculation of short-term erosion rates that are among the highest obtained for our study region, we also found ample evidence for aeolian deposition, and particularly so when coupled with upwind fluvial sand supplies. Aeolian transport however, is dependent on a number of factors,

including the presence of a stable or increasing sand supply, favorable wind direction, and lack of topographic and vegetative barriers. Mitigation of site erosion, for example by aeolian sand gully annealing, therefore requires a sequential combination of events, all of which may or may not occur when expected. In this study, aeolian deposition, even with anthropogenic forcing via fluvial sand-bar building high flow dam releases, was found to be generally insufficient to offset the effects of precipitation-induced gullying. However, we note that fluvially-connected aeolian deposition is a time-dependent process, the outer limit of which may extend for many years.

Acknowledgements—The LiDAR change detection and meteorological data for this paper are available through open-access United States Geological Survey (USGS) reports (Collins *et al.*, 2009, 2012; Draut *et al.*, 2009a, 2009b, 2010b; Dealy *et al.*, 2014; Hazel *et al.*, 2010; Hereford *et al.*, 1993, 2014) and also summarized in Supplementary Information Table S2. Infiltration data used in our analyses is provided in Supplementary Information Table S1 and associated references (i.e. O'Brien *et al.*, 2009b; Pederson *et al.*, 2003).

Funding for this research was provided by the USGS Grand Canyon Monitoring and Research Center, in cooperation with the US Bureau of Reclamation. The authors thank G. O'Brien and J. Pederson (Utah State University, Logan, UT), A. Draut (USGS, Santa Cruz, CA), and J. Hazel (Northern Arizona University, Flagstaff, AZ) for making their raw infiltration, precipitation, grain size, and sand bar data available for analysis. T. Dealy (USGS, Flagstaff, AZ) and E. Phillips (USGS, Menlo Park, CA) assisted with preliminary precipitation data analysis and K. Brown, B. Fisher, and K. Kohl (USGS, Flagstaff, AZ) provided survey support for the LiDAR fieldwork. J. DiLeo (USGS, Menlo Park, CA) drafted Figure 1. The authors also thank A. Draut (USGS, Santa Cruz, CA), K. Schmidt (USGS, Menlo Park, CA), V. Holliday (University of Arizona, Tucson, AZ), and five anonymous reviewers for providing comments on earlier drafts of this manuscript. Any use of trade, firm, or product names is for descriptive purposes only and does not imply endorsement by the US Government.

Appendix

Rainfall–runoff numerical model description

This section presents detailed information on the numerical model described in the 'Numerical modeling' section and used to obtain overland flow routing results presented in the 'Verification with rainfall–runoff model results' section and Figures 3 and 8A. Additional validation and explanation can be found in Bedford (2008).

Runoff model equations

The runoff model consists of a distributed implementation of two-dimensional shallow overland flow equations coupled with interactive one-dimensional infiltration over site domains with high-resolution grid cells (generally 10 to 25 cm per side). When possible, input parameters were based on maps determined from field sampling. Other parameters were based on published values for similar environments, and a simple calibration was used to constrain and validate these choices.

In the model, overland flow and infiltration through time are described by the diffusion wave approximation of the Saint Venant equations (Richardson and Julien, 1994). Mass continuity is defined by:

$$\frac{\partial h}{\partial t}+\frac{\partial q_x}{\partial x}+\frac{\partial q_y}{\partial y}=r-i \tag{A1}$$

where h is flow depth (L), t is time (T), q is unit discharge (L^2/T), x and y are spatial dimensions (L), r is rainfall rate (L/T), and i is the infiltration rate (L/T). Unit discharge is calculated as:

$$q_x = uh \text{ and } q_y = vh \tag{A2}$$

where u and v are the vertically averaged flow velocity (L/T) in the x- and y-dimensions, respectively. Average depth-integrated velocity is computed from the Darcy–Weisbach equation:

$$v=\sqrt{\frac{8g\ h\ S_f}{ff}} \tag{A3}$$

where g is the acceleration due to gravity (L/T^2), S_f is the friction slope, and ff is the Darcy–Weisbach friction factor. The diffusion wave approximation is used, in which the friction slope is determined by the water surface. This technique allows water to be ponded behind complex microtopography, which will affect runoff determinations, and can play an important role in infiltration. The surface flow is assumed to be fully turbulent, which is likely for the modeled domain because field observations indicate that flow rarely outlasts rainfall, and raindrop disturbance creates turbulent conditions.

One-dimensional infiltration is computed using the Green–Ampt equation, following the form of Esteves *et al.* (2000),

$$i_{cap}=K_{eff}\left(\frac{Z_i+h+\Psi_{wf}}{Z_i}\right) \tag{A4}$$

where i_{cap} is the infiltration capacity (L/T) at any time, K_{eff} is the effective ($< K_{sat}$) hydraulic conductivity (L/T), Ψ_{wf} is the effective wetting front soil suction (L), and Z_i is the wetting front depth, computed as:

$$Z_i=\frac{I}{\theta_s-\theta_i} \tag{A5}$$

where I is the cumulative infiltration at the given time step (L), θ_s is the saturated water content (L^3/L^3), and θ_i is the initial water content (L^3/L^3).

The actual infiltration rate at any time, i, is computed by:

$$i = i_{cap} \text{ for } (r+Q_{in}) > i_{cap} \tag{A6a}$$

$$i = r+Q_{in} \text{ for } (r+Q_{in}) < i_{cap} \tag{A6b}$$

where Q_{in} is the run-on discharge given by: $Q_{in}=(q_x+q_y)/dx$ when q_x and q_y are constrained as positive values and dx is the cell size.

Boundary conditions and numerical implementation

'No flow' boundary conditions are imposed on the upper and side boundaries of the model domain, which mimics the upper boundary conditions of the field sites and simplifies the solution without loss of accuracy for the side boundaries due to the large model domain (sides measuring hundreds of meters). Lower boundary conditions are imposed using the kinematic wave equation on a positively (downward) sloping plane 1.2-times the slope of the lowest grid cells. This lower boundary condition was selected to avoid ponding of surface water along the lower boundary and because it mimics the field setting.

Numerical computations are implemented using a forward-differencing, finite-difference scheme on a staggered grid. That is, the model calculate fluxes at model cell boundaries and flow depths and infiltration at the cell centers. Numerical stability is established using the Courant condition, with a Courant coefficient of 0.1 as described in Howes *et al.* (2006). Newton–Raphson iteration is used to determine convergence of the Green–Ampt equation.

References

Ahmad MF, Dong P, Mamat M, Wan Nik WB, Mohd MH. 2011. The critical shear stresses for sand and mud mixture. *Applied Mathematical Sciences* **5**(2): 53–71.

Bedford DR. 2008. *Effects of Vegetation-related Soil Heterogeneity on Runoff, Infiltration, and Redistribution in Semi-arid Shrubland and Grassland Landscapes*, PhD Dissertation, University of Colorado, Boulder, CO. http://gradworks.umi.com/33/37/3337180.html

Belnap J 2006. The potential roles of biological soil crust in dryland hydrologic cycles. *Hydrological Processes* **20**: 3159–3178. DOI:10.1002/hyp.6325.

Belnap J, Munson SM, Field JP. 2011. Aeolian and fluvial processes in dryland regions: the need for integrated studies. *Ecohydrology* **4**: 615–622. DOI:10.1002/eco.258.

Billingsley GH. 2000. *Geologic map of the Grand Canyon 30′ × 60′ Quadrangle, Coconino and Mohave Counties, Northwestern Arizona*, US Geological Survey Geologic Investigations Series I-2688: map+pamphlet. http://pubs.usgs.gov/imap/i-2688/

Blackburn WH. 1975. Factors influencing infiltration and sediment production of semiarid rangelands in Nevada. *Water Resources Research* **11**(6): 929–937.

Bouwer H 1966. Rapid field measurement of air entry value and hydraulic conductivity of soil as significant parameters in flow system analysis. *Water Resources Research* **2**(4): 729–738. DOI:10.1029/WR002i004p00729.

Breshears DD, Whicker JJ, Johansen MP, Pinder JE. 2003. Wind and water erosion and transport in semi-arid shrubland, grassland and forest ecosystems: quantifying dominance of horizontal wind-driven transport. *Earth Surace Processes and Landforms* **28**: 1189–1209. DOI:10.1002/esp.1034.

Bullard JE, Livingstone I. 2002. Interactions between aeolian and fluvial systems in dryland environments. *Area* **34**(1): 8–16. DOI:10.1111/1475-4762.00052.

Bullard JE, McTainsh GH. 2003. Aeolian-fluvial interactions in dryland environments: examples, concepts and Australia case study. *Progress in Physical Geography* **27**(4): 471–501. DOI:10.1191/0309133303pp386ra.

Caine N 1980. The rainfall intensity-duration control of shallow landslides and debris flows. *Geografiska Annaler, Series A, Physical Geography* **62**(1/2): 23–27.

Canfield HE, Lopes VL, Goodrich DC. 2001. Hillslope characteristics and particle size composition of surficial armoring on a semiarid watershed in the southwestern. *United States: Catena* **44**(1): 1–11.

Cantón Y, Solé-Benet A, de Vente J, Boix-Fayos C, Calvo-Cases A, Asensio C, Puigdefábregas J. 2011. A review of runoff generation and soil erosion across scales in semiarid south-eastern Spain. *Journal of Arid Environments* **75**(12): 1254–1261.

Castillo VM, Gomez-Plaza A, Martinez-Mena M. 2003. The role of antecedent soil water content in the runoff response of semiarid catchments: a simulation approach. *Journal of Hydrology* **284**(1–4): 114–130.

Collins BD, Minasian D, Kayen R. 2009. *Topographic Change Detection at Select Archaeological Sites in Grand Canyon National Park, Arizona, 2006–2007*, US Geological Survey Scientific Investigations Report 2009-5116. http://pubs.usgs.gov/sir/2009/5116/

Collins BD, Corbett SC, Fairley HC, Minasian D, Kayen R, Dealy TP, Bedford DR. 2012. *Topographic change detection at select archaeological sites in Grand Canyon National Park, Arizona, 2007–2010*, US Geological Survey Scientific Investigations Report 2012-5133. http://pubs.usgs.gov/sir/2012/5133/

Davis PA, Mietz SN, Kohl KA, Rosiek MR, Gonzales FM, Manone MF, Hazel JE, Kaplinski MA. 2002. Evaluation of LiDAR and photogrammetry for monitoring volume changes in riparian resources within the Grand Canyon, Arizona. In *Proceedings of the Pecora 15/Land Satellite Information IV/ISPRS Commission I/FIEOS 2002 Conference*. http://www.isprs.org/proceedings/XXXIV/part1/paper/00028.pdf

Dealy TP, East AE, Fairley HC. 2014. *2010 Weather and Aeolian Sand-transport Data from the Colorado River Corridor, Grand Canyon, Arizona, US Geological Survey Open-File Report 2014–1135*. http://dx.doi.org/10.3133/ofr20141135.

Deganutti MA, Marchi L, Arattano M. 2000. Rainfall and debris-flow occurrence in the Moscardo basin (Italian Alps). In *Debris-flow Hazard Mitigation – Mechanics, Prediction, and Assessment – Proceedings of the 2nd International Conference on Debris-Flow Hazards Mitigation*, Wieczorek GF, Naeser ND (eds). Balkema: Rotterdam; 67–72.

Drakos PG, Reneau SL. 2007. Episodic aeolian events and preservation of mesa top archaeological sites on the Pajarito Plateau, New Mexico. In *New Mexico Geological Society Guidebook, 58th Field Conference, Geology of the Jemez Mountains Region II*, 121–130.

Draut AE. 2012. Effects of river regulation on aeolian landscapes, Colorado River, USA. *Journal of Geophysical Research* **117**: F02022. DOI:10.1029/2011JF002329.

Draut AE, Rubin DM. 2008. *The Role of Aeolian Sediment in the Preservation of Archaeological Sites along the Colorado River Corridor Grand Canyon National Park, Arizona*, US Geological Survey Professional Paper 1756. http://pubs.usgs.gov/pp/1756

Draut AE, Rubin DM, Dierker JL, Fairley HC, Griffiths RE, Hazel JE, Jr, Hunter RE, Kohl K, Leap LM, Nials FL, Topping DJ, Yeatts M. 2008. Application of sedimentary-structure interpretation to geoarchaeological studies in the Colorado River corridor, Grand Canyon, Arizona, USA. *Geomorphology* **101**: 497–509. DOI:10.1016/j.geomorph.2007.04.032.

Draut AE, Andrews T, Fairley HC, Brown CR. 2009a. *2007 Weather and Aeolian Sand-transport Data from the Colorado River Corridor, Grand Canyon, Arizona*, US Geological Survey Open–File Report 2009-1098. http://pubs.usgs.gov/of/2009/1098/

Draut AE, Sondossi HA, Hazel Jr JE, Fairley HC, Andrews T, Brown CR, Vanaman KM. 2009b. *2008 Weather and Aeolian Sand-transport Data from the Colorado River Corridor, Grand Canyon, Arizona*, US Geological Survey Open-File Report 2009-1190. http://pubs.usgs.gov/of/2009/1190/

Draut AE, Hazel Jr JE, Fairley HC, Brown CR. 2010a. Aeolian reworking of sandbars from the March 2008 Glen Canyon Dam high-flow experiment in Grand Canyon. In *Proceedings of the Colorado River Basin Science Resource Management Symposium*, Melis TS, *et al.* (eds), US Geological Survey Scientific Investigations Report 2010-5135. http://pubs.usgs.gov/sir/2010/5135/

Draut AE, Sondossi HA, Dealy TP, Hazel Jr JE, Fairley HC, Brown CR. 2010b. *2009 Weather and Aeolian Sand-transport Data from the Colorado River Corridor, Grand Canyon, Arizona*, US Geological Survey Open-File Report 2010-1166. http://pubs.usgs.gov/of/2010/1166/

Dunne T 1978. Field studies of hillslope flow processes. In *Hillslope Hydrology*, Kirkby MJ (ed). Wiley: London; 227–293.

Dunne T, Black RD. 1970a. An experimental investigation of runoff production in permeable soils. *Water Resources Research* **6**(2): 478–490. DOI:10.1029/WR006i002p00478.

Dunne T, Black RD. 1970b. Partial-area contributions to storm runoff in a small New England watershed. *Water Resources Research* **6**(5): 1296–1311. DOI:10.1029/WR006i005p01296.

Esteves M, Faucher X, Galle S, Vauclin M. 2000. Overland flow and infiltration modelling for small plots during unsteady rain: numerical results versus observed values. *Journal of Hydrology* **228**(3–4): 265–282. DOI:10.1016/S0022-1694(00)00155-4.

Fairley HC. 2003. *Changing River: Time, Culture and the Transformation of Landscape in the Grand Canyon*, a regional research design for the study of cultural resources along the Colorado River in lower Glen Canyon and Grand Canyon National Park, Arizona, Technical Series 79. Statistical Research, Inc.: Tucson, AZ; 179 pp.

Fairley HC. 2005. Cultural resources in the Colorado River corridor. In *The State of the Colorado River Ecosystem in Grand Canyon*, Gloss SP, Lovich JE, Melis TS (eds), US Geological Survey Circular 1282. US Geological Survey: Reston, VA; 177–192. http://pubs.usgs.gov/circ/1282/.

Fairley HC, Bungart PW, Coder CM, Huffman J, Samples TL, Balsom JR. 1994. *The Grand Canyon River Corridor Survey Project; Archaeological Survey along the Colorado River between Glen Canyon Dam and Separation Canyon, Grand Canyon National Park*, Report submitted to the Bureau of Reclamation, cooperative agreement No. 9AA-40-07920. Bureau of Reclamation: Flagstaff, AZ.

Fitzjohn C, Ternan JL, Williams AG. 1998. Soil moisture variability in a semi-arid gully catchment: implications for runoff and erosion control. *Catena* **32**(1): 55–70.

Freeze RA. 1972. Role of subsurface flow in generating surface runoff: 2. Upstream source areas. *Water Resources Research* **8**(5): 1272–1283. DOI:10.1029/WR008i005p01272.

García MH. 2008. Sediment transport and morphodynamics. In *Sedimentation Engineering: Processes, Measurements, Modeling, and Practice*, García M (ed.). ASCE: Reston, VA; 121–163. DOI. 10.1061/9780784408148.ch02

Gardner TW, Jorgensen DW, Shuman C, Lemieux CR. 1987. Geomorphic and tectonic process rates: effects of measured time interval. *Geology* **15**(3): 259–261. DOI:10.1130/0091-7613(1987)15<259:GATPRE>2.0.CO;2.

Gibling MR, Sinha R, Roy NG, Tandon SK, Jain M. 2008. Quaternary fluvial and eolian deposits on the Belan river, India: paleoclimatic setting of Paleolithic to Neolithic archaeological sites over the past 85,000 years. *Quaternary Science Reviews* **27**(3–4): 391–410.

Grayson RB, Moore ID, McMahon TA. 1992. Physically based hydrologic modeling: 1. A terrain-based model for investigative purposes. *Water Resources Research* **28**(10): 2639–2658. DOI:10.1029/92WR01258.

Guzzetti F, Peruccacci S, Rossi M, Stark CP. 2008. The rainfall intensity–duration control of shallow landslides and debris flows: an update. *Landslides* **5**: 3–17. DOI:10.1007/s10346-007-0112-1.

Harris EC. 1989. *Principles of Archaeological Stratigraphy* (2nd edition). Academic Press: London.

Hazel Jr JE, Kaplinski M, Parnell RA, Fairley HC. 2008. *Aggradation and Degradation of the Palisades Gully Network, 1996 to 2005, with Emphasis on the November 2004 High-flow Experiment, Grand Canyon National Park, Arizona*. US Geological Survey Open-File Report 2008-1264. http://pubs.usgs.gov/of/2008/1264/

Hazel Jr JE, Grams PE, Schmidt JC, Kaplinski M. 2010. *Sandbar Response in Marble and Grand Canyons, Arizona, following the 2008 High-flow Experiment on the Colorado River*, US Geological Survey Scientific Investigations Report 2010-5015. http://pubs.usgs.gov/sir/2010/5015/

Hereford R, Fairley HC, Thompson KS, Balsom JR. 1993. *Surficial Geology, Geomorphology and Erosion of Archeologic Sites along the Colorado River, Eastern Grand Canyon, Grand Canyon National Park, Arizona*, US Geological Survey Open-File Report 93-517. US Geological Survey: Reston, VA.

Hereford R, Burke KJ, Thompson KS. 2000. *Map Showing Quaternary Geology and Geomorphology of the Granite Park Area, Grand Canyon, Arizona*, US Geological Survey Geologic Investigations Series I–2662. http://pubs.usgs.gov/imap/i2662/

Hereford R, Bennett GE, Fairley HC. 2014. *Precipitation Variability of the Grand Canyon Region, 1893 through 2009, and its Implications for Studying Effects of Gullying of Holocene Terraces and Associated Archaeological Sites in Grand Canyon, Arizona*, US Geological Survey Open-File Report 2014–1006. http://dx.doi.org/10.3133/ofr20141006

Holliday VT, Hoffecker JF, Goldberg P, Macphail RI, Forman SL, Anikovich M, Sinitsyn A. 2007. Geoarchaeology of the Kostenki–Borshchevo sites, Don River Valley, Russia. *Geoarchaeology* **22**: 181–228. DOI:10.1002/gea.20163.

Horton RE. 1945. Erosional development of streams and their drainage basins: hydrophysical approach to quantitative morphology. *Geological Society of America Bulletin* **56**(3): 275–370. DOI:10.1130/0016-7606(1945)56.

Howard A, Dolan R. 1981. Geomorphology of the Colorado River in the Grand Canyon. *Journal of Geology* **89**(3): 269–298.

Howes DA, Abrahams AD. 2003. Modeling runoff and runon in a desert shrubland ecosystem, Jornada Basin, New Mexico. *Geomorphology* **53**: 45–73.

Howes DA, Abrahams AD, Pitman EB. 2006. One- and two-dimensional modelling of overland flow in semiarid shrubland, Jornada basin, New Mexico. *Hydrological Processes* **20**(5): 1027–1046. DOI:10.1002/hyp.5922.

Jett SC. 1968. Grand Canyon dams, split-twig figurines, and 'hit-and-run' archaeology. *American Antiquity* **33**(3): 341–351.

Julien PY, Simons DB. 1985. Sediment transport capacity of overland flow. *Transactions of the ASAE* **28**(3): 755–762.

Kean JW, Staley DM, Leeper RJ, Schmidt KM, Gartner JE. 2012. A low-cost method to measure the timing of postfire flash floods and debris flows relative to rainfall. *Water Resources Research* **48**: W05516. DOI:10.1029/2011WR011460.

Kidron GJ. 2007. Millimeter-scale microrelief affecting runoff yield over microbiotic crust in the Negev Desert. *Catena* **70**: 266–273.

Kirchner JW, Dietrich WE, Iseya F, Ikeda H. 1990. The variability of critical shear stress, friction angle, and grain protrusion in water-worked sediments. *Sedimentology* **37**: 647–672.

Kirkby MJ, Bracken LJ. 2009. Gully processes and gully dynamics. *Earth Surface Processes and Landforms* **34**: 1841–1851. DOI:10.1002/esp.1866.

Kurc SA, Small EE. 2004. Dynamics of evapotranspiration in semiarid grassland and shrubland ecosystems during the summer monsoon season, central New Mexico. *Water Resources Research* **40**: W09305. DOI:10.1029/2004WR003068.

Magirl CS, Breedlove MJ, Webb RH, Griffiths PG. 2008. *Modeling Water-surface Elevations and Virtual Shorelines for the Colorado River in Grand Canyon, Arizona*, US Geological Survey Scientific Investigations Report 2008-5075. http://pubs.usgs.gov/sir/2008/5075/

Martínez G, Martínez GA. 2011. Late Holocene environmental dynamics in fluvial and aeolian depositional settings: archaeological record variability at the lower basin of the Colorado river (Argentina). *Quaternary International* **245**(1): 89–102.

Melis TS (ed.). 2011. *Effects of Three High-flow Experiments on the Colorado River Ecosystem Downstream from Glen Canyon Dam, Arizona*, US Geological Survey Circular 1366. http://pubs.usgs.gov/circ/1366/

Mirus BB, Loague K. 2013. How runoff begins (and ends): characterizing hydrologic response at the catchment scale. *Water Resources Research* **49**(5): 2987–3006. DOI:10.1002/wrcr.20218.

Morris DA, Johnson AI. 1967. *Summary of Hydrologic and Physical Properties of Rock and Soil Materials, as Analyzed by the Hydrologic Laboratory of the U.S. Geological Survey, 1948–60*, US Geological Survey Water Supply Paper 1839-D. http://pubs.usgs.gov/wsp/1839d/report.pdf

Nickling WG, Neuman CM. 2009. Aeolian sediment transport. In *Geomorphology of Desert Environments*, Parsons AJ, Abrahams AD (eds). Springer: Dordrecht; 517–555.

National Oceanic and Atmospheric Administration (NOAA). 2013. *Daily Summaries Station Details for Lees Ferry 1916–2012* (*Station GHCND:USC00024849*) *and Phantom Ranch 1935–2013* (*Stations GHCND:USC00024335 and GHCND:USC00026471*). NOAA, National Climatic Data Center, Climate Data Online. http://www.ncdc.noaa.gov/cdo-web/ [10 October 2013].

O'Brien G, Pederson J. 2009a. *Geomorphic Attributes of 232 Cultural Sites along the Colorado River in Grand Canyon National Park, Arizona*, Utah State University report submitted to USGS Grand Canyon Monitoring and Research Center. http://www.gcmrc.gov/publications/library.aspx

O'Brien G, Pederson J. 2009b. *Gully Erosion Processes and Parameters at Six Cultural Sites along the Colorado River Corridor in Grand Canyon National Park, Arizona*, Utah State University report submitted to USGS Grand Canyon Monitoring and Research Center. http://www.gcmrc.gov/publications/library.aspx

Okin GS, Gillette DA, Herrick JE. 2006. Multi-scale controls on and consequences of aeolian processes in landscape change in arid and semi-arid environments. *Journal of Arid Environments* **65**: 253–275.

Pederson JL, Petersen PA, Macfarlane WW, Gonzales MF, Kohl K. 2003. *Mitigation, Monitoring, and Geomorphology Related to Gully Erosion of Cultural Sites in Grand Canyon*, Utah State University report submitted to USGS Grand Canyon Monitoring and Research Center. http://www.gcmrc.gov/library/reports/cultural/Archaeology/Pederson2003.pdf

Pederson JL, Petersen PA, Dierker JL. 2006a. Gullying and erosion control at archaeological sites in Grand Canyon, Arizona. *Earth Surface Processes and Landforms* **31**(4): 507–525. DOI:10.1002/esp.1286.

Pederson JL, Anders MD, Rittenour TM, Sharp WD, Gosse JC, Karlstrom KE. 2006b. Using fill terraces to understand incision rates and evolution of the Colorado River in eastern Grand Canyon, Arizona. *Journal of Geophysical Research (Earth Surface)* **111**: F02003. DOI:10.1029/2004JF000201.

Pederson JL, O'Brien G, Neff T, Spurr K, Damp J, Collette J, Suart G, Purcell D. 2011. *Grand Canyon Geoarchaeology Project: Report on Data Recovery at Nine Cultural Sites in Grand Canyon and Lower Glen Canyon, 2008–2010*, Utah State University report submitted to the Bureau of Reclamation, Upper Colorado River Region, Salt Lake City, Utah, September 2011.

Powell JW. 1875. *The Exploration of the Colorado River of the West and Its Tributaries*. US Government Printing Office: Washington, DC.

Prosser IP, Slade CJ. 1994. Gully formation and the role of valley-floor vegetation, southeastern Australia. *Geology* **22**(12): 1127–1130. DOI:10.1130/0091-7613(1994)022<1127:GFATRO>2.3.CO;2.

Ravi S, Breshears DD, Huxman TE, D'Odorico P. 2010. Land degradation in drylands: Interactions among hydrologic–aeolian erosion and vegetation dynamics. *Geomorphology* **116**(3–4): 236–245. DOI:10.1016/j.geomorph.2009.11.023.

Richardson JR, Julien PY. 1994. Suitability of simplified overland flow equations. *Water Resources Research* **30**(3): 665–671. DOI:10.1029/93WR03098.

Ritchie JC, Nearing MA, Nichols MA, Ritchie CA. 2005. Patterns of soil erosion and redeposition on Lucky Hills Watershed, Walnut Gulch Experimental Watershed, Arizona. *Catena* **61**(2–3): 122–130. DOI:10.1016/j.catena.2005.03.012.

Rodríguez-Caballeroa E, Cantón Y, Chamizo S, Afana A, Solé-Benet A. 2012. Effects of biological soil crusts on surface roughness and implications for runoff and erosion. *Geomorphology* **145–146**: 81–89. DOI:10.1016/j.geomorph.2011.12.042.

Roskin J, Katra I, Porat N, Zilberman E. 2013. Evolution of Middle to Late Pleistocene sandy calcareous paleosols underlying the northwestern Negev Desert Dunefield (Israel). *Palaeogeography, Palaeoclimatology, Palaeoecology* **387**: 134–152. DOI:10.1016/j.palaeo.2013.07.018.

Roskin J, Katra I, Agha N, Goring-Morris AN, Porat N, Barzilai O. 2014. Rapid anthropogenic response to short-term aeolian-fluvial palaeoenvironmental changes during the Late Pleistocene-Holocene transition in the northern Negev Desert, Israel. *Quaternary Science Reviews* **99**: 176–192. DOI:10.1016/j.quascirev.2014.06.018.

Sankey JB, Draut AE. 2014. Gully annealing by aeolian sediment: field and remote-sensing investigation of aeolian–hillslope–fluvial interactions, Colorado River corridor, Arizona, USA. *Geomorphology* **220**(1): 68–80.

Schwartz DW. 1965. Nankoweap to Unkar: An archaeological survey of the upper Grand Canyon. *American Antiquity* **30**(3): 278–296.

Smith RE. 2002. *Infiltration Theory for Hydrologic Applications – Water Resources Monograph 15*. AGU: Washington, DC. DOI. 10.1029/WM015

Taylor WW. 1958. *Two Archaeological Studies in Northern Arizona*: *The Pueblo Ecology Study*: *Hail and Farewell and a Brief Survey through the Grand Canyon of the Colorado River – Bulletin 30*. Northern Arizona Society of Science and Art: Flagstaff, AZ.

Thompson KS, Potochnik AR (eds). 2000. Development of a Geomorphic Model to Predict Erosion of Pre-dam Colorado River Terraces Containing Archaeological Resources, SWCA Cultural Resources Report 99-257. http://www.gcmrc.gov/publications/library.aspx

Topping DJ, Rubin DM, Vierra LE, Jr. 2000. Colorado River sediment transport 1– natural sediment supply limitation and the influence of Glen Canyon Dam. *Water Resources Research* **36**: 515–542. DOI:10.1029/1999WR900285.

Topping DJ, Schmidt JC, Vierra Jr LE. 2003. *Computation and Analysis of the Instantaneous-discharge Record for the Colorado River at Lees Ferry, Arizona—May 8, 1921, through September 30, 2000*, US Geological Survey Professional Paper 1677. http://pubs.usgs.gov/pp/pp1677/

Tucker GE, Arnold L, Bras RL, Flores H, Istanbulluoglu E, Sólyom P. 2006. Headwater channel dynamics in semiarid rangelands, Colorado high plains, USA. *GSA Bulletin* **118**(7–8): 959–974. DOI:10.1130/B25928.1.

Wainwright J 1994. Erosion of archaeological sites: Results and implications of a site simulation mode. *Geoarchaeology* **9**: 173–201. DOI:10.1002/gea.3340090302.

Waters MR. 1997. *Principles of Geoarchaeology*: *A North American Perspective*. University of Arizona Press: Tucson, AZ.

Webb RH, Griffiths PG, Melis TS, Hartley DR. 2000. *Sediment Delivery by Ungaged Tributaries of the Colorado River in Grand Canyon, Arizona*, US Geological Survey Water-Resources Investigations Report 2000-4055. http://www.gcmrc.gov/library/reports/Physical/Coarse_Sed_Webb/WRIR2000_00-4055s.pdf

Wright SA, Melis TS, Topping DJ, Rubin DM. 2005. Influence of Glen Canyon Dam operations on downstream sand resources of the Colorado River in Grand Canyon. In *The State of the Colorado River Ecosystem in Grand Canyon*, Gloss SP, Lovich JE, Melis TS (eds), US Geological Survey Circular 1282. US Geological Survey: Reston, VA; 17–31. http://pubs.usgs.gov/circ/1282/.

Zhang Y-G, Nearing MA, Liu BY, Van Pelt RS, Stone JJ, Wei H, Scott RL. 2011. Comparative rates of wind versus water erosion from a small semiarid watershed in southern Arizona, USA. *Aeolian Research* **3**(2): 197–204. DOI:10.1016/j.aeolia.2011.03.006.

Supporting information

Additional supporting information may be found in the online version of this article at the publisher's web site.